University of South-Eastern Norway

www.usn.no

FMH606 Master's Thesis 2022

Process Technology

The impact of waste heat recovery unit installation on the operation and control of the raw meal department at Norcem Brevik

Fredrik Kasin Høibjerg

Faculty of Technology, Natural sciences and Maritime Sciences

Campus Porsgrunn

University of South-Eastern Norway

www.usn.no

Course: FMH606 Master's Thesis, 2022

Title: The impact of waste heat recovery unit installation on the operation and control of the raw meal department at Norcem Brevik

Number of pages: 100

Keywords: CO_2 capture, cement production, system modeling, Maple

Student: Fredrik Kasin Høibjerg

Supervisor: Lars Andre Tokheim

External partner: Norcem Brevik

Summary:

As a step towards net-zero emissions in the future, a CO_2 capture facility is under construction at the cement plant Norcem in Brevik. This will reduce emissions by 400 000t/yr. To utilize waste heat from the cement production a waste heat recovery unit will be installed in the raw meal department, utilizing the available waste heat from the kiln preheater. With altered temperatures and flow rates, this report will seek to find the impact of these changes on the production capacity.

For normal WHRU operation, the production capacity should not be affected since the needed temperatures and flow rates are available. The challenge will be in controlling the pressures to reach the desired flow rates and the corresponding temperatures.

With the reduced water content in the flue gas from the preheater, the saturation temperature will be reduced. This will in turn allow for a reduction in the mill inlet temperature and recovery of an additional 1.92MW of heat. This is dependent on sufficient residence time for the raw materials to reach complete evaporation of water.

Further, the work has investigated the impact of ambient air leaking into the process and how the removal of this would impact the system. Results indicate that complete will cause a hot gas deficit and is therefore not an option. Partially sealing the system will allow for an additional 2.4MW of heat recovered during LA production. For STD the sealing will only cause increased outlet temperatures and no further heat recovery will be possible.

Preface

By this, I present to you the thesis written during my last semester studying Process Technology at the University in South-Eastern Norway (USN). This thesis is written to fulfill the graduation requirements, and the work took place from January to June 2022.

The project was done in collaboration with Norcem AS, which has also been my employer for the last 10 years. It has been a demanding task but through extensive work, results have been gathered and knowledge acquired. Under steady guidance from my supervisor, professor Lars Andre Tokheim, this work has let me develop my skills and knowledge, and for that, I am forever grateful.

For my colleagues that have been supporting me during this entire process, with valuable data and useful discussions, I convey my sincere gratitude.

Lastly, I would like to extend my utmost gratitude to my patient family that has supported me throughout my educational endeavors over the last 5 years.

Porsgrunn, 18.5.2022

Fredrik Kasin Høibjerg

Contents

Nomenclature

Abbreviation	Description
AFM	Aerofall mill
AMLAS	Raw meal composition controller
BF	Bag filter
$CaCO_3$	Limestone
CCS	Carbon capture and storage
CEMS	Continuous emissions monitoring system
CO_2	Carbon dioxide
ESP	Electrostatic precipitator
FA	False air
GCT	Gas conditioning tower
H_2O	Water
HGF	Hot gas fan
ID fan	Main process fan
LA	Low alkali raw meal
N_2	Nitrogen
O_2	Oxygen
RH	Relative humidity
RM	Raw materials
STD	Standard raw meal
WHRU	Waste heat recovery unit

Symbol	Units	Description
α	[#]	Pitot tube factor
ΔH_{vap}	$[kJ/kg]$	Latent heat of vaporization
Δp	$[mbar]$	Differential pressure for velocity calculation
ΔT	$[°C]$	Estimated gas and solids temperature difference
ΔT_{RH}	$[°C]$	The temperature difference between dew point and operating temperature
η_{BF}	[%]	Bag filter efficiency
η_{Cyc}	[%]	Cyclone efficiency
η_{ESP}	[%]	Electrostatic precipitator efficiency
η_{FAN}	[%]	Centrifugal fan efficiency
η_{Sep}	[%]	Coarse separator efficiency
$\langle Cp \rangle$	$[kJ/kgK]$	Mean specific heat capacity
A_{AFM}	$[m^2]$	Mill surface area
A_{Cyc}	$[m^2]$	Cyclones surface area
A_{Sep}	$[m^2]$	Separator surface area
Cp_g	$[kJ/kgK]$	Specific heat capacity of the gas
Cp_{FA}	$[kJ/kgK]$	Specific heat capacity of the false air
Cp_{RM}	$[kJ/kgK]$	Specific heat capacity of the raw materials
h_c	$[kW/m^2K]$	Convective heat transfer coefficient
MM	$[kg/mol]$	Molar mass of a substance
m_{H_2O}	$[g]$	Water collected in gas sampling

$\dot{m}_{g,i}$	$[kg/h]$	Gas mass flow[1]
$\dot{m}_{FA,i}$	$[kg/h]$	False air mass flow[1]
$\dot{m}_{RM,i}$	$[kg/h]$	Raw material mass flow rate[1]
$\dot{m}_{H_2O,vap}$	$[kg/h]$	Vapor mass flow
P_{ID}	$[kW]$	AFM main fan power input
P_{mill}	$[kW]$	Mill motor power input
p_{abs}	$[mbar]$	Absolute pressure for velocity calculations
p_{H_2O}	$[mmHG]$	The partial pressure of water
p_N	$[Pa]$	Normal pressure
$Q_{Loss,AFM}$	$[kW]$	AFM surface heat loss
$Q_{Loss,Cyc}$	$[kW]$	Cyclones surface heat loss
$Q_{Loss,Sep}$	$[kW]$	Coarse separator surface heat loss
R	$[kJ/kmolK]$	Universal gas constant
T_i	$[°C]$	Gas temperatures[1]
T_A	$[°C]$	Ambient air temperature
T_{avg}	$[°C]$	Average temperature
T_N	$[°C]$	Normal temperature
T_m	$[°C]$	Measured temperature
T_s	$[°C]$	Surface temperature
$T_{RM,i}$	$[°C]$	Raw material and solids temperature[1]
V_{mol}	$[L/mol]$	Standard molar volume

[1] i representing stream number

VP_{H_2O}	$[mmHG]$	Vapor pressure of water
$\dot{V}_{g,i}$	$[Nm^3/h]$	Normal volumetric gas flow[1]
$\dot{V}_{FA,i}$	$[Nm^3/h]$	Normal volumetric false air flow[1]
$\dot{V}_{H_2O,vap}$	$[Nm^3/h]$	Normal volumetric flow rate of evaporated water
$\dot{V}_{m,ref}$	$[Nm^3/h]$	Measured normal volumetric flow
v	[m/s]	Velocity
v_{Con}	[m/s]	Coarse separator belt speed
$w_{RM,Con}$	[kg/m]	Weighed materials on coarse separator belt
w_{H_2O}	[%]	Weight fraction of water in raw materials
$y_{H_2O,i}$	[%]	Water volume fraction in the gas[1]
$y_{O_2,FA}$	[%]	Oxygen volume fraction in false air
$y_{O_2,i}$	[%]	Oxygen volume fraction in the gas[1]

List of figures

List of tables

1 Introduction

1.1 Background

Cement production is worldwide one of the biggest contributors to CO_2 emissions, standing for approximately 5-7% of the global emissions. This is due to the energy requirements for producing clinker and the release of CO_2 bound up in the limestone. In total, approximately 50% of the emissions stem from the decarbonization of limestone, 40 % from the burning of clinker, and 10% from the remaining processes[1]. To counter these emissions and to get in line with the Paris agreement the industry must act.

In Norway, Norcem with its two plants is the only cement producer. At the plant located in Brevik, the capacity is roughly 1 million tons of clinker per year and 1.2 million tons of cement, with an annual release of 800 kilotons of CO_2[2]. To handle these emissions and reduce the impact per ton of clinker produced several steps have been implemented over the years. Amongst these are the reduction of clinker used in the final cement, where this is replaced with ash from coal-fired powerplants and limestone powder. As seen in Figure 1.1 the yearly emissions per ton of cement produced have decreased over the last decade.

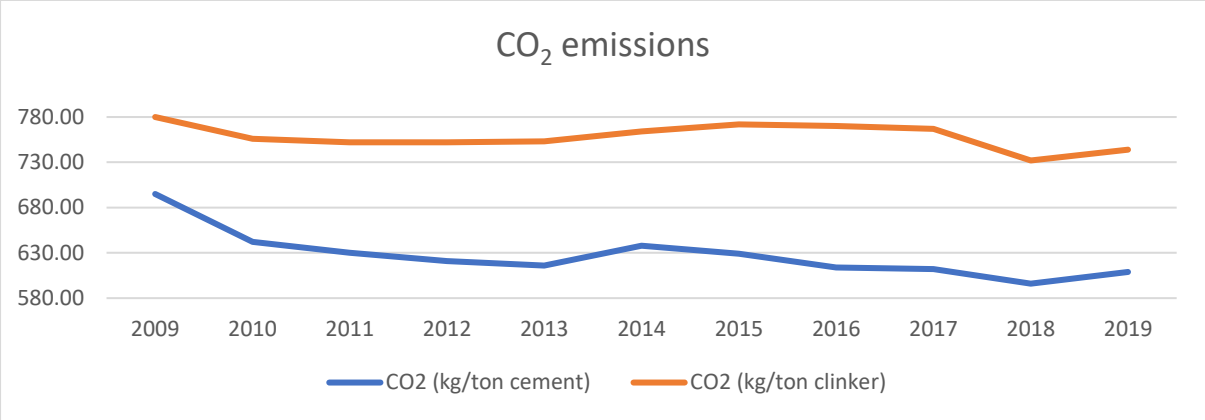

Figure 1.1 CO2 emission/ton produced[2]

But the reductions in emissions from lowering the clinker ratio in the final product and moving from fossil- to alternative fuels can only take us so far. The CO_2 bound up in the limestone is an unavoidable source that must be tackled differently. As of today, one possible solution is the carbon capture and storage technology (CCS), which is currently under construction at the Brevik plant. This is a costly and technology-intensive process that requires large investments with high energy demands. The chosen technology in Brevik is the amine-based absorption process, where CO_2 is absorbed by the amine solution in an absorption column. This is a reversible reaction, and the CO_2 is released again by heating the rich amine solution to 120°C. After this separation lean amine is then reused in the absorber.

To reduce the operational costs related to energy demands the waste heat available in the flue gases is to be utilized. This is achieved by installing waste heat recovery units (WHRU) on the flue gas lines to produce steam for the regeneration of the amine solution in the capture plant. In Brevik, three WHRUs will be installed, with one being installed in the raw meal department. This installation will affect the operability of the process with changes in flow rates, temperatures, and H_2O content in the flue gas.

1.2 Objectives

The object of this work is to clarify how the WHRU installation will affect the drying- and production capacity of the raw meal department. To answer this, several sub-tasks are listed below

1. Identify flow rates, temperatures, and gas compositions in the system today, and see how they will change after the WHRU installation.
2. Ambient air leaking into the process, so-called false air, is a highly relevant topic today and must be addressed in this work. Can the reduction of false air justify an investment to seal the production equipment?
3. With the WHRU in operation the system will operate at a higher inlet temperature with lower H_2O content in the flue gas. This will change the drying capacity and must be investigated.
4. Finally, the operational constraints limiting the production are to be identified.

The complete task description is found in Appendix A.

1.3 Methods

To answer the key questions in this work several datasets and calculations are needed. To obtain this the following methods are used

1. Data collection from the plant control system, e.g. flow rates, temperatures, flue gas composition, and pressures.
2. A mass, energy, and component balance must be developed for the system, both existing and planned.
3. Based on the data collection and developed balance measurements must be performed to collect the remaining needed data, both for supplying the model and for validation of model results.

1.4 Report Structure

Chapter 2 will describe the system and give the reader a basic understanding of the processes involved in the production of raw meal. It will also seek to put the process in context with the rest of the production, and describe the CCS modifications along with the controllability of the plant.

Chapter 3 describes the mathematical model developed for the system and how the model is extended for the WHRU. Mass, heat, and component balances that are used will be presented, and other relevant relations.

Chapter 4 presents all the measurements that are done in this work, including the methods used and the results.

Chapter 5 describes how the model is solved and presents the output. Results are compared with measured values for validation and for ensuring reliable data before the model is used for the WHRU system. The following cases are solved

- STD and LA production today
- STD and LA production with WHRU in operation
- STD and LA production with WHRU in operation and mill inlet sealed and partially sealed for false air intrusion
- STD and LA production with WHRU in operation with reduced temperatures based on lower saturation temperatures

Chapter 6 will discuss the overall results and seek to further validate the results.

Chapter 7 presents the conclusion on the main objectives stated in the thesis project description.

2 System Description

In this chapter, the process and production of raw meal will be presented. The reader should get a basic understanding of the process and vital parameters, present, and future.

2.1 Present process description

The raw meal is produced through crushing, mixing, and grinding of several raw materials to a fine powder. This powder will make up the raw meal that is burnt in a rotary kiln downstream to form clinker, with all the necessary minerals. This formation is ensured by controlling the limestone and other additives to achieve a homogenous mix with the proper qualities. Norcem mainly produces two types of raw meal, namely the standard mix (STD) and low-alkali mix (LA), depending on the product quality produced in the kiln.

2.1.1 Raw materials

The main ingredient in the raw meal is limestone and in Brevik, there are three types in use. Dalen type, which is mined underground in Brevik, Bjorntvedt from an open quarry located in Porsgrunn, and Verdal which is shipped to the plant from a quarry in Trondelag. These types vary in quality with Dalen, and Verdal having a calcium carbonate (CaCO3) content of 88% and the highest quality. Bjorntvedt has a lower CaCO3 content and is used for blending with Dalen and Verdal.

To reach the final product quality and ensure mineral formation in the kiln, several additives are added to the mix. Today Norcem Brevik uses quartz as a silica source, copper ore as an iron source, and a waste product from the metal industry called Norox as an aluminum source. Other additives are gypsum and slag. All these materials are ground to a fine meal and blended in homogenization silos to reach a homogenous mixture.

For producing STD and LA raw meals, different amounts of limestone and additives are needed such that the recipe will change. Typical raw material mass percentages, according to recipes, are shown in Table 2.1.

Table 2.1 Raw meal constituents

Quality	**STD**	**LA**
Dalen/Verdal Limestone	55.8	88.6
Bjorntvedt Limestone	41.3	0
Quartz	1.31	5.9
Gypsum	0.8	
Copper Ore	0.7	3.46

Slag		2.05

In Figure 2.1 on page 17 the process is illustrated with a flowsheet where all the different streams are numbered. Important equipment is labeled to simplify referencing in the report. Orange lines indicate hot gas flow, raw material/solid streams are indicated with black lines whilst red lines are used for false air streams.

A 3D model of the system is found in Appendix B where the equipment, separation, and mixing points are indicated. Model created by the CCS project team.

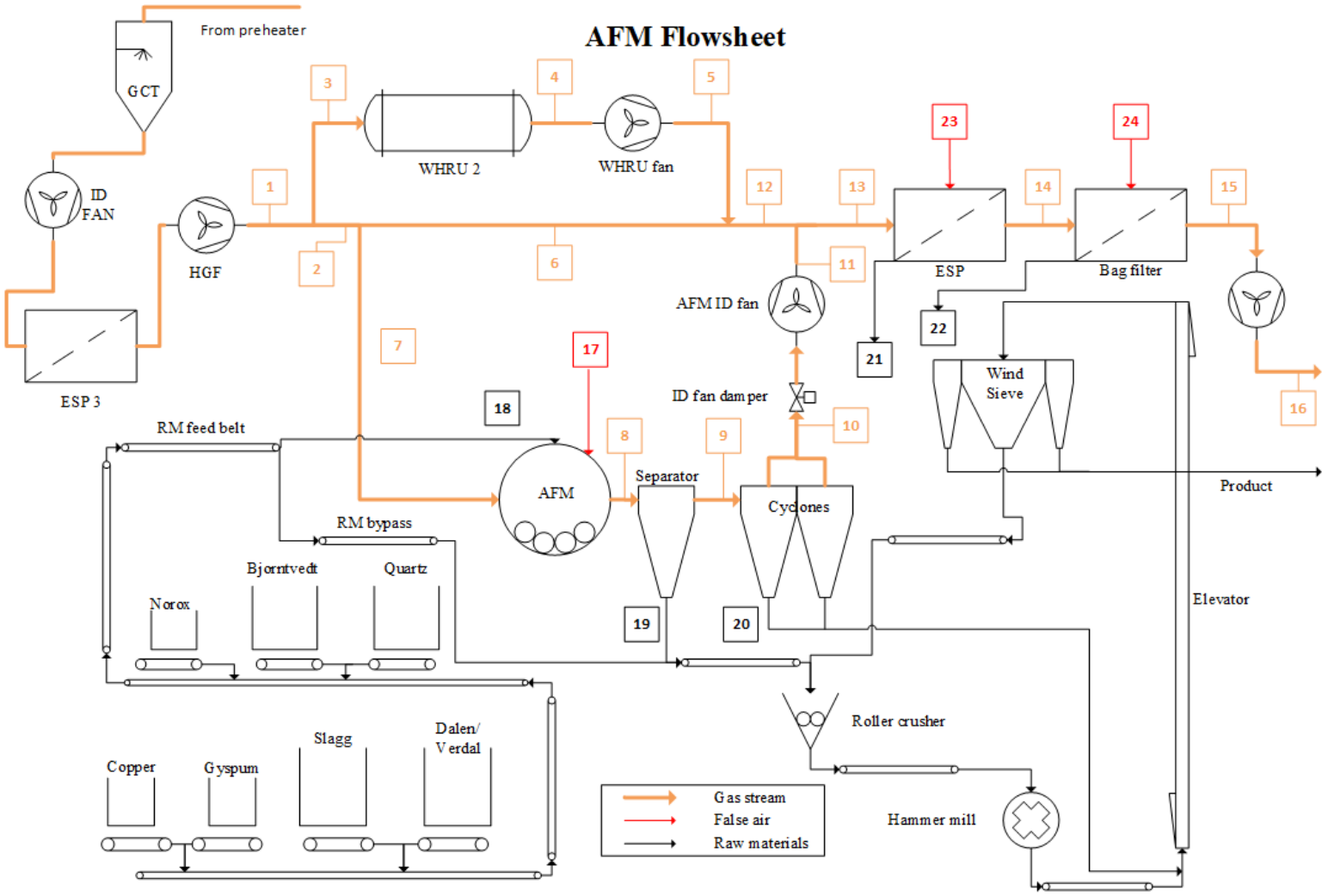

Figure 2.1 Flowsheet with stream identification

2.1.2 Dosing and grinding of raw materials

To achieve the needed quality the constituents of the raw meal are carefully analyzed. This is done by an online analyzing system, Full Stream Analyzer, installed on the final conveyor belt before the mill. This system analyzes the composition of the materials continuously and corrects the ratio of the raw materials according to the recipe every 7 minutes through changes in feed rates. These changes are done with weigh belt feeders installed for each material type below the silo outlet.

After weighing and analyzing the materials are fed into the Aero-fall mill (AFM) where they are crushed to fine gravel and dust. This mill is a, 10m in diameter and 2m long, rotating ball mill where the balls are lifted as the mill rotates and crush the materials as they fall again. In addition to crushing, the mill will dry the materials as hot gas from the kiln is used to transport the crushed materials out of the mill. By adjusting the flow rate of this hot gas, the degree of filling in the mill and the fineness of the materials exiting the mill can be controlled. This is done by opening or closing a damper downstream of the mill.

After the ball mill the crushed materials are carried over to the separator chamber, often referred to as the coarse separator. This is a gravity settler, where the particles are separated from the horizontally flowing gas by gravity. To enhance this separation the volume increases, and the flow velocity is reduced. Coarse particles will exit the separator through the bottom on a conveyor belt where they are transported to the roller press. After the coarse separator, the gas will pass through two parallel cyclones for further separation of fines and finally exit the process through an electrostatic precipitator and a bag filter.

In the roller press, the materials will pass two hydraulic rollers and be crushed further, before the flattened materials are broken up in the hammer mill. After this process, the materials are fine enough to be transported to the wind sieve.

2.1.3 Sieving and homogenization

The wind sieve is a dynamic separator where the materials are fed laterally into to top section and distributed uniformly by a rotating distributor disc. Through trajectory separation, the coarse and fine particles will split, and the fine inner material will meet a recirculating and upwards flowing stream of air that will entrain the finest particles and transport them to the cyclones. The fineness of this raw meal can be adjusted in two ways, by changing the speed on the distributor disc or adjusting the quantity of air recirculating in the sieve.

The finished product will be transported to silos for homogenization and storage. For transport, a system using 4 blow tanks ensures continuous transportation of the raw meal to the homogenization silos. Here the finished raw meal is buffered and mixed by aeration. The final homogenized product is then transported in air slides to the final storage silos.

2.1.4 Hot gas stream from the kiln system

Waste heat from clinker production is utilized in raw meal production for drying out the materials. This gas has passed through the kiln system and preheater before being transported

to the raw meal department. In Figure 2.2 the gas flow for standard raw meal production with key temperatures, for both STD and LA production, is shown.

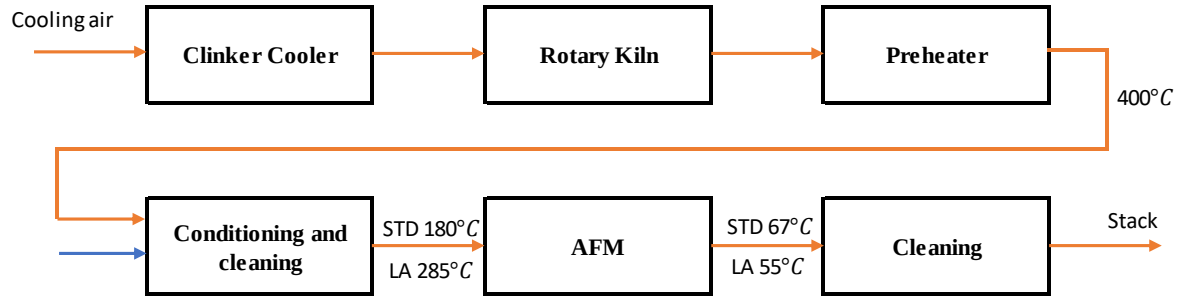

Figure 2.2 Gas flow overview

The flue gas exiting the preheater is cooled to a specified temperature in the conditioning tower by spraying it with water in a co-current direction. The cooled gas is then cleaned in ESP3 before being transported to the raw meal department. Gas transportation is achieved with two radial centrifugal fans, with the preheater ID fan located after the GCT, and the hot gas fan located in the raw meal department.

The flue gas consists mainly of nitrogen, carbon dioxide, oxygen, and water. From here on described by their abbreviations. Typical gas composition is shown in Table 2.2.

Table 2.2 Flue gas components for STD production[3]

Gas composition	Units	Preheater exit	Downstream GCT
H_2O	[%]	9.0	22.2
O_2	[%]	4.6	5.2
CO_2	[%]	23.5	18.4
N_2	[%]	62.9	54.2

Due to the cooling of the gas by water injection in the GCT the H_2O concentration in the gas increases. This fraction will vary with the GCT outlet temperature, and for LA production, with a higher temperature, will be reduced.

2.1.5 Hot gas stream in the AFM department

Upon entering the raw meal department, downstream the hot gas fan, the hot gas stream is separated into two streams. One stream enters the AFM and the second stream bypasses the

mill and is transported directly to the ESP and bag filter for purification. By doing this the amount of gas entering the AFM can be controlled and tuned for each raw meal type produced.

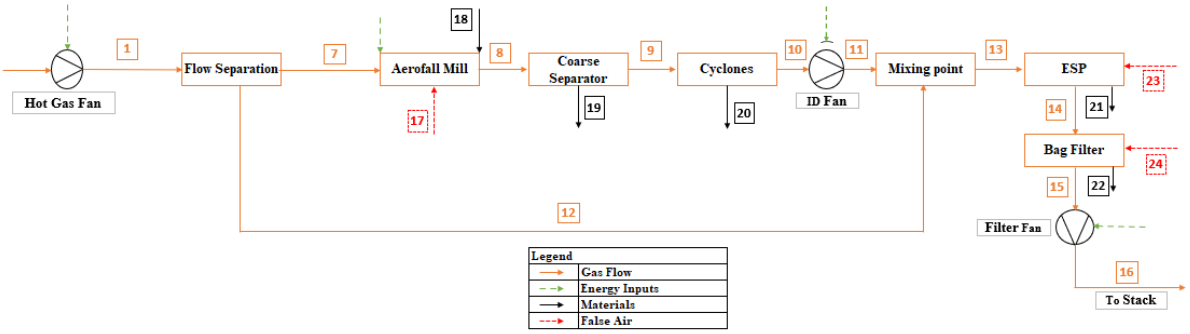

Figure 2.3 Streams AFM

In Figure 2.3 the gas stream is shown together with the material-, false air- and energy streams.

2.1.6 Controllability of present raw meal production

To control and stabilize the operation of the AFM the temperature and gas flow rate must be controlled. In this way, the degree of filling in the mill is controlled and the material going out has sufficient residence time in the mill. To ensure stable operation these parameters must be controlled:

1. The flow rate must be sufficient to carry materials out of the mill over to the coarse separator and cyclones.
2. Temperature after the AFM must be sufficiently high to prevent condensation in equipment downstream.
3. Negative pressure at AFM inlet to prevent gas leaking into the environments

These parameters will change with what type of raw meal is produced due to changes in composition and grindability of the different raw materials, with the type of limestone having the biggest impact on performance. Bjorntvedt limestone is hard to grind, hence a longer residence time in the mill is needed, compared to the softer Dalen/Verdal limestone. In Table 2.1 the typical composition of STD and LA is shown, and as LA contains no Bjorntvedt this mix will grind easily and vice versa. To compensate for these variations two control schemes are implemented:

1. ID fan damper to adjust the gas flow rate through the mill. Increasing or decreasing damper opening is done manually from the control room and will affect the size distribution of particles carried out of the mill as well as the total amount.
2. The degree of filling in the mill is automatically adjusted by changing the raw material feed to the mill while maintaining the feed composition.

By increasing the damper opening, the gas flow through the mill will increase, hence the material carry-over will increase. A too big opening will cause an excessive carry-over

resulting in overloading of the equipment downstream, i.e. the roller crusher and the wind sieve. A too low opening will in turn cause an unnecessary reduction in production rate due to the AFM filling up. The degree of filling inside the mill is measured with an electronic ear, and variations in this level are compensated by adjusting the raw material feed to the mill. The degree of filling is controlled by experience and is often a trade-off between production capacity and wear on mill lining.

An increase in the damper opening will successively lower the mill inlet pressure. This will directly affect the false air intake with the following reduction in mill outlet temperature. This in turn leads to the second important parameter, the mill outlet temperature. To prevent condensation downstream this must be kept above 52°C by controlling the temperature of the gas entering the mill. This is mainly adjusted by decreasing or increasing the amount of water injected in the GCT which will change the gas temperature entering the raw meal department. This will further affect the H_2O concentration in the gas, as seen in Table 2.2, and alter the saturation temperature. In addition, the H_2O fraction in the raw materials varies from <1% in limstone to 17% in Norox.

Thirdly, a negative pressure must be maintained upstream of the AFM to prevent kiln flue gas from entering the surroundings. This is automatically controlled by adjusting the filter fan speed which in turn will affect the bypass/AFM flow rate ratio. A higher fan speed will give a lower pressure upstream of the AFM in the separation point and reduce the gas available for the AFM. This will be somewhat compensated with false air, with the following mill outlet temperature reduction. The pressure upstream of the AFM is typically operated in the range of -0.2 to -1.5mbar.

2.1.7 Changeover conditions

When the production is changed from one type to another, the operational values and parameters will change. In Figure 2.4 pressures upstream of the AFM and the bypass duct illustrates a shift in the gas flow. By increasing the opening of the ID fan damper, the gas flow through the mill increases. Bypass-duct static pressure rises as the flow velocity decreases and mill inlet static pressure drops as the velocity increases. This is visualized further by the increase in fan amps. In Figure 2.5 the temperatures decrease as the temperature from the GCT is lowered. The spikes seen downstream of the mill are caused by the loss of material feed.

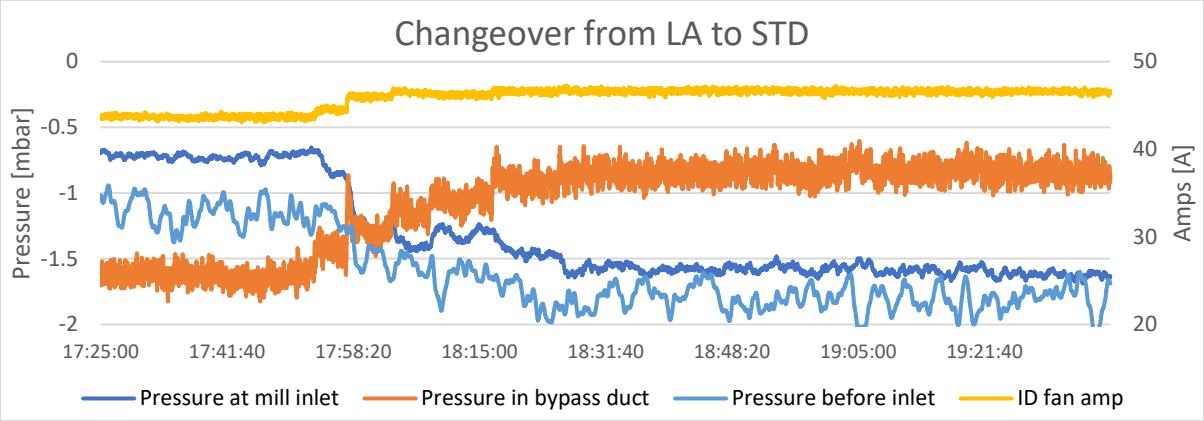

Figure 2.4 Pressures during a changeover from LA to STD

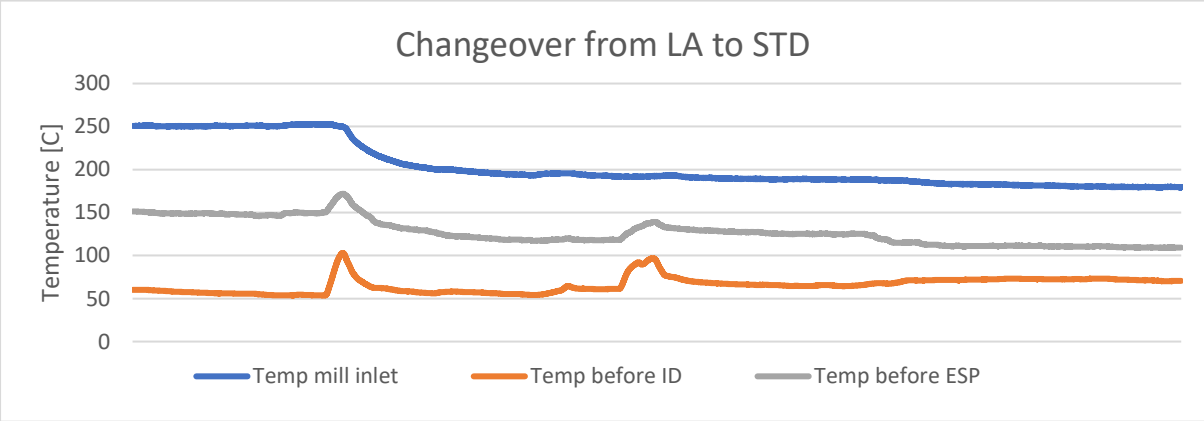

Figure 2.5 Temperatures during a changeover from LA to STD

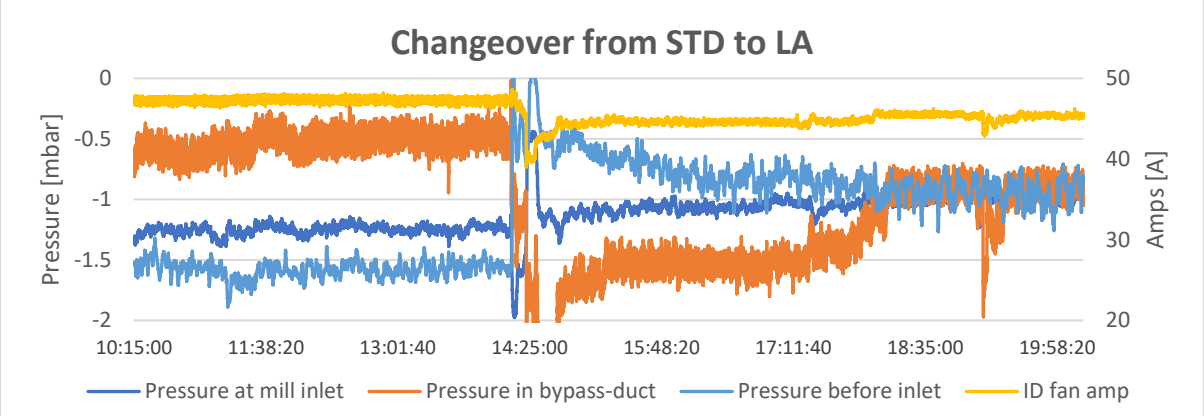

Figure 2.6 Pressures during a changeover from STD to LA

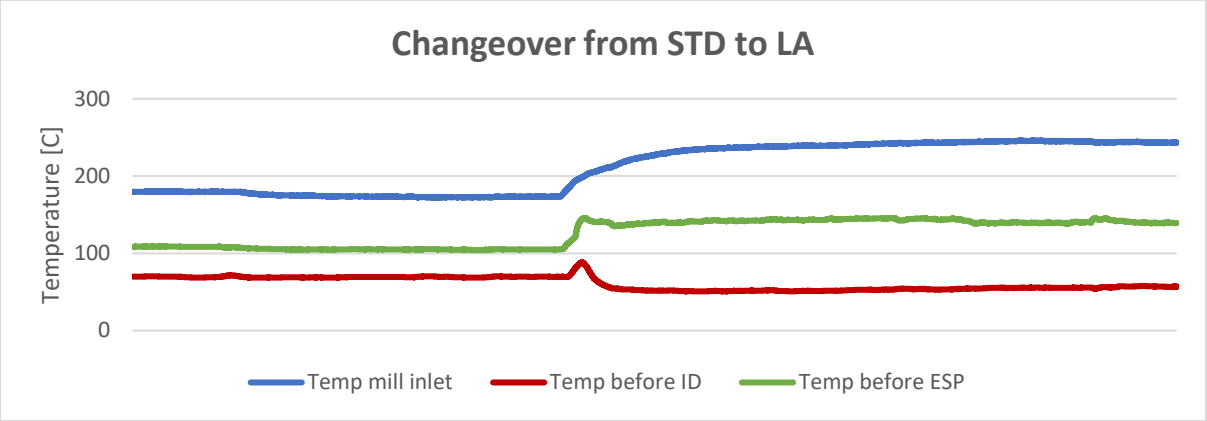

Figure 2.7 Temperatures during a changeover from STA to LA

In Figure 2.6 and Figure 2.7 the conditions during the changeover from STD to LA are shown. From the reduced temperature upstream of the ID fan a reduced flow of hot gas through the mill is interpreted. This is further proved by the temperature rise downstream of the fan, caused by the increased hot gas flow through the bypass duct. This supports the operational principles of a lesser gas flow during LA production to prevent too large of a material carry-over. When changing from LA to STD the temperature curves will show an opposite pattern as the main gas stream is passing through the mill.

2.1.8 Temperature sensitivity

The rate of solids carry-over from the AFM to the coarse separator is a function of gas velocity, but production capacity is reported to decrease with increasing temperatures. To see how it affected this capacity a test was performed over 12 hours, during STD production. The temperature was raised from 180 to 220°C out of the GCT resulting in a rise in AFM inlet temperature to 215°C. All other parameters were kept constant to maintain the absolute gas flow rate. The AFM outlet temperature increased from 70 to 81°C. With this increase in temperature, a decrease in the ID fan amps was seen, likely due to the reduced gas mass flow. The temperature was kept at this level for approximately 6 hours before returning to 180°C. Overall the results indicated that the grinding performance does not seem to change with increasing temperature, at least within the normal operating range.

2.2 Heat recovery and operability

This chapter will present modifications done to the raw meal production process during the CCS installation period. These modifications will alter temperatures, pressures, and flow rates such that the operation of the facility overall will change.

2.2.1 WHRU installation

To utilize the heat available in the kiln flue gas a waste heat recovery unit is being installed in the raw meal department. This is a shell and tube boiler producing steam for the amine

regeneration in the capture plant. The unit will be installed outside the existing raw meal department and draw gas downstream of the hot gas fan and return it to the existing bypass duct. The flow through the unit is controlled by the WHRU fan and to ensure proper guidance of gas flow at the connection point, the diameter is increased to lower the flow velocity. In Figure 2.8 the WHRU installation is included in the AFM flow sheet, where “Flow separation 1” indicates the first connection point and “Flow mixing 1” is the boiler outlet connection point. Upstream the raw meal department a crossover duct is installed to bleed off approximately 20 000Nm^3/h to preheater string 1.

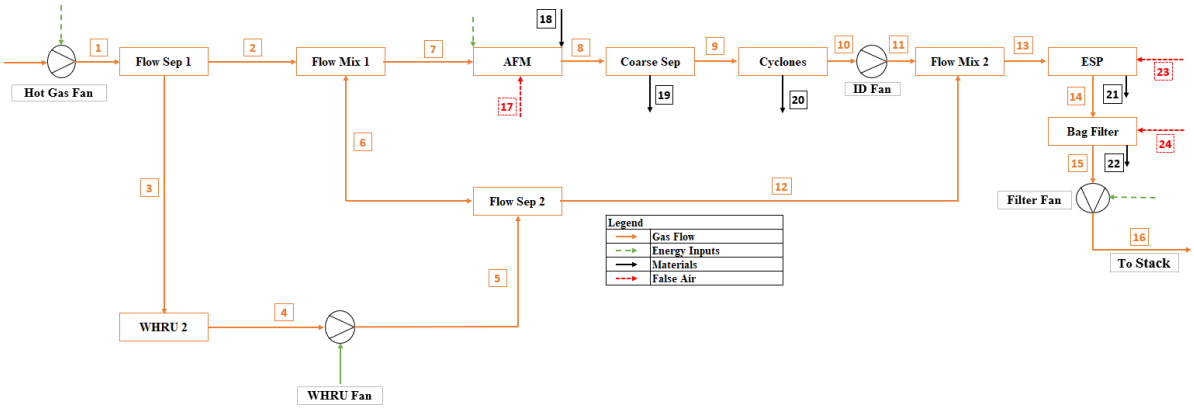

Figure 2.8 Streams after WHRU installation

2.2.2 Process alterations

With the WHRU in operation, the need to utilize all available heat from the preheater is essential. To achieve this, no water will be injected into the GCT and the temperature in the raw meal department inlet will increase to approximately 360°C. This temperature is too high to be used in the AFM and must be controlled to not overheat the mill system. This is done by redirecting the gas through the WHRU where the temperature is reduced from 360 to 170°C. For STD production all the gas can be redirected through the WHRU, whilst for LA production, with the higher temperature demand, a fraction of the hot inlet gas must be routed directly to the mill. WHRU fan speed will be adjusted to shift the gas direction and flow rate to the current production need.

2.2.3 Operational risk with higher temperatures

With the increased inlet temperature in the raw meal department comes the risk of overheating the system with unintended shutdowns of the WHRU. With a sudden stop of the recovery unit, the mill will handle the initial temperature rise, but the bag filter will trip and bypass the gas. This will result in an unwanted plume of dust to the environment through the stack. To prevent this it is necessary to immediately start water injection in the GCT to cool down the gas to below 230°C.

Anyhow, due to the thermal energy stored in the ducts and ESP 3, there will be a delayed response time on the temperature. This response time needs to be small enough to be able to

buffer the heat in the WHRU until sufficient cooling is achieved. In Figure 2.9 the temperature is plotted where the delayed response time is seen. In the future scenario, the temperature must be brought down from 360°C to a temperature that will prevent the gas temperature in stream 14 to surpass 250°C. If the response time from the GCT is to slow additional measures should be implemented.

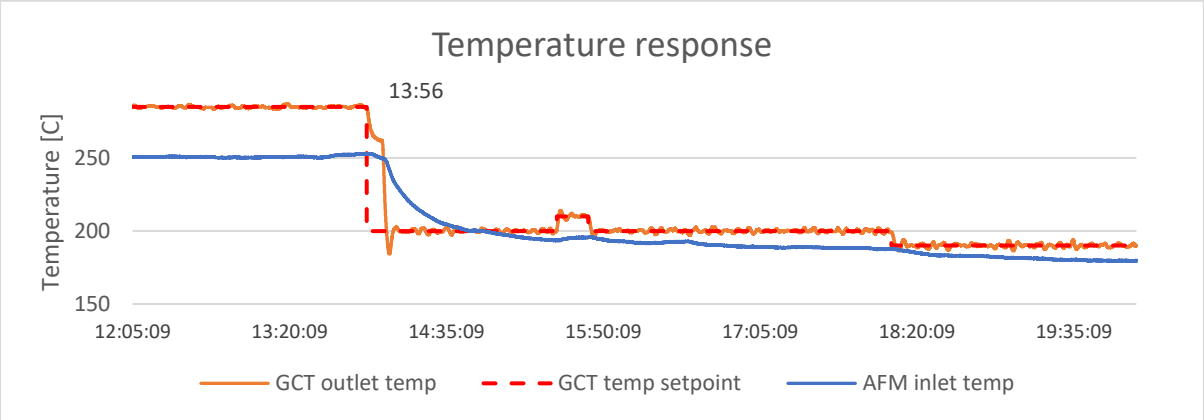

Figure 2.9 Temperature response

2.3 False air intrusion

False air intrusion is the leaking of ambient air into the process streams at negative pressure. This will raise the energy consumption due to the low ambient air temperature and the increased flow rates that must be compensated for with higher fan speeds. With this, increased wear and need for maintenance are expected along with increased energy costs.

Ambient air intrusion at the mill inlet is the biggest contributor to false air in the raw meal department. This is caused by the large openings needed for the raw material feed installation. Materials are fed directly into the mill by a belt conveyor, with minimal sealing to the atmosphere. Other sources at the mill inlet are the burner opening, cracks, and hatches for cleaning purposes. The total false air flow rate will highly depend on the mill inlet pressure which is operated at levels ranging from -0.3 to -1.5mbar, with a lower pressure causing a higher flow rate.

A lesser amount of false air is expected in the filters, with the BF being the biggest contributor due to 8 chambers with in- and outlet ducting.

The total flow rate into the system will be calculated in the model based on O_2 concentrations, from both manual measurements and online analyzers.

3 Mathematical Model

To describe the system the following mathematical model is developed. This is used to calculate parameters important in the process operability such as false air intrusion, drying capacity, and how the installation of the WHRU will affect this capacity. The system is solved using mass-, component-, and energy balances. Initially, the model is developed based on the current system and then extended to include the WHRU installation.

3.1 Assumptions

The following assumptions were made to develop and solve the model

1. Assuming ideal gas
2. Gas composition is simplified by only evaluating N_2, O_2, CO_2, and H_2O.
3. Chemical reactions are neglected.
4. Assuming constant efficiencies in bag filter, ESP, cyclones, and coarse separator.
5. The H_2O content in the raw material feed is kept constant.
6. Raw material specific heat capacity is based on only limestone and kept constant between STD and LA
7. The moisture content of solids exiting the process is assumed to be zero.
8. Raw material feed to the AFM is reduced by 60t/h for STD and 10t/h for LA as finer particles are separated and bypassed the AFM.
9. Heat loss in the insulated ducts is assumed to be zero.
10. False air intrusion is assumed to occur only at the AFM inlet and in the ESP and BF.
11. Constant atmospheric pressure within the model

3.2 Balances

The different balances used in solving the system are introduced in this chapter. These equations are describing the existing system for both STD and LA production. All streams are numbered as given in Figure 2.3.

3.2.1 Mass balance

The mass balance is done for both gas- and material streams. In equation (3.1) the total gas balance is given. The total false air balance is given in equation (3.2).

$$\dot{m}_{g,16} = \dot{m}_{g,1} + \dot{m}_{FA} + \dot{m}_{H_2O,vap} \tag{3.1}$$

$$\dot{m}_{FA} = \dot{m}_{FA,17} + \dot{m}_{FA,23} + \dot{m}_{FA,24} \tag{3.2}$$

Equation (3.3) is describing the gas separation in the first separation point. Here the needed gas is guided to the AFM in stream 7, whilst excess gas is passing through the bypass duct.

$$\dot{m}_{g,2} = \dot{m}_{g,7} + \dot{m}_{g,6} \tag{3.3}$$

In the AFM gas stream 7 is mixed with false air from the mill inlet and water vapor from the raw materials. This balance is given in equation (3.4). From the mill, the flow rate remains unchanged until the mixing point downstream of the mill system, where the mass balance is given in equation (3.5).

$$\dot{m}_{g,8} = \dot{m}_{g,7} + \dot{m}_{FA,17} + \dot{m}_{H_2O,vap} \tag{3.4}$$

$$\dot{m}_{g,13} = \dot{m}_{g,11} + \dot{m}_{g,12} \tag{3.5}$$

For the ESP and bag filter, the mass balance is given in equation (3.6) and equation (3.7), respectively.

$$\dot{m}_{g,15} = \dot{m}_{g,14} + \dot{m}_{FA,24} \tag{3.6}$$

$$\dot{m}_{g,14} = \dot{m}_{g,13} + \dot{m}_{FA,23} \tag{3.7}$$

In addition to the mass balances, the following relationships define the system, in equations (3.6) to (3.11).

$$\dot{m}_{g,8} = \dot{m}_{g,9} \tag{3.8}$$

$$\dot{m}_{g,9} = \dot{m}_{g,10} \tag{3.9}$$

$$\dot{m}_{g,10} = \dot{m}_{g,11} \tag{3.10}$$

$$\dot{m}_{g,15} = \dot{m}_{g,16} \tag{3.11}$$

For the solid materials, the balances in equations (3.12) to (3.15) are describing the system.

$$\dot{m}_{RM,15} = \dot{m}_{RM,14} - \dot{m}_{RM,22} \tag{3.12}$$

$$\dot{m}_{RM,14} = \dot{m}_{RM,13} - \dot{m}_{RM,21} \tag{3.13}$$

$$\dot{m}_{RM10,} = \dot{m}_{RM,9} - \dot{m}_{RM,20} \tag{3.14}$$

$$\dot{m}_{RM9,} = \dot{m}_{RM,8} - \dot{m}_{RM,19} \tag{3.15}$$

With the additional relationships given in equations (3.16) to (3.19).

$$\dot{m}_{RM,18} = \left(1 - w_{H_2O}\right) * \dot{m}_{RM,8} \tag{3.16}$$

$$\dot{m}_{RM,10} = \dot{m}_{RM,11} \tag{3.17}$$

$$\dot{m}_{RM,11} = \dot{m}_{RM,13} \tag{3.18}$$

$$\dot{m}_{RM,15} = \dot{m}_{RM,16} \tag{3.19}$$

3.2.2 Energy balances

For the AFM, the total energy balance is given in equation (3.20). Balances for the separator and cyclones are given in equations (3.21) and (3.22), respectively.

$$\begin{aligned} &\dot{m}_{g,7} * Cp_{g,7} * (T_7 - T_8) + P_{mill} \\ &\quad = \left(\dot{m}_{RM,18} * \left(1 - w_{H_2O,18}\right)\right) * Cp_{RM} * \left(T_{RM,8} - T_{RM,18}\right) \\ &\quad + \dot{m}_{RM,18} * w_{H_2O,15} * \left(Cp_{H_2O,vapor} * \left(T_8 - T_{RM,18}\right) + \Delta H_{vap}\right) \\ &\quad + \dot{m}_{FA,17} * Cp_{FA} * (T_8 - T_A) + Q_{Loss,AFM} \end{aligned} \tag{3.20}$$

$$\begin{aligned} &\dot{m}_{g,8} * Cp_{g,8} * (T_8 - T_9) \\ &\quad = \dot{m}_{RM,19} * Cp_{RM,19} * \left(T_{RM,19} - T_{RM,8}\right) + \dot{m}_{RM,9} * Cp_{RM,9} \\ &\quad * \left(T_{RM,9} - T_{RM,8}\right) + Q_{Loss,Sep} \end{aligned} \tag{3.21}$$

$$\begin{aligned} &\dot{m}_{g,9} * Cp_{g,9} * (T_9 - T_{10}) \\ &\quad = \dot{m}_{RM,20} * Cp_{RM,20} * \left(T_{RM,20} - T_{RM,9}\right) \\ &\quad + \dot{m}_{RM,10} * Cp_{RM,10} * \left(T_{10} - T_{RM,9}\right) + Q_{Loss,Cyc} \end{aligned} \tag{3.22}$$

Downstream of the mill system, in the mixing point the cooled mill gas is mixed with the warmer bypassed gas stream. This balance is given in equation (3.23).

$$\dot{m}_{g,12} * Cp_{g,12} * (T_{12} - T_{13}) = \dot{m}_{g,11} * Cp_{g,11} * (T_{13} - T_{11}) \quad (3.23)$$

For the ESP and bag filter the energy balance is given in equations (3.24) and (3.25).

$$\dot{m}_{g,13} * Cp_{g,avg} * (T_{12} - T_{13}) = \dot{m}_{FA,23} * Cp_{FA} * (T_{14} - T_A) \quad (3.24)$$

$$\dot{m}_{g,14} * Cp_{g,avg} * (T_{14} - T_{15}) = \dot{m}_{FA,24} * Cp_{FA} * (T_{15} - T_A) \quad (3.25)$$

In addition, the relationships given in equation (3.26) and (3.27) is used to solve the system.

$$T_1 = T_7 \quad (3.26)$$

$$T_1 = T_{12} \quad (3.27)$$

3.2.3 Component balances

For O_2 the total balance is given in equation (3.28) and for H_2O in equation (3.29). CO_2 total balance is given in equation (3.30).

$$y_{O_2,16} * \dot{V}_{g,16} = y_{O_2,1} * \dot{V}_{g,1} + y_{O_2,FA} * \dot{V}_{FA} \quad (3.28)$$

$$y_{H_2O,16} * \dot{V}_{g,16} = y_{H_2O,1} * \dot{V}_{g,1} + \dot{V}_{H_2O,vap} \quad (3.29)$$

$$y_{CO_2,16} * \dot{V}_{g,16} = y_{CO_2,1} * \dot{V}_{g,1} \quad (3.30)$$

The AFM O_2 and H_2O balance are given in equations (3.31) and (3.32). CO_2 concentration is calculated using equation (3.33) and by that defining the composition in streams 8 to 11.

$$y_{O_2,8} * \dot{V}_{g,8} = y_{O_2,7} * \dot{V}_{g,7} + y_{O_2,FA} * \dot{V}_{FA,AFM,17} \quad (3.31)$$

$$y_{H_2O,8} * \dot{V}_{g,8} = y_{H_2O,7} * \dot{V}_{g,7} + \dot{V}_{H_2O,vap} \quad (3.32)$$

$$y_{CO_2,8} * \dot{V}_{g,8} = y_{CO_2,7} * \dot{V}_{g,7} \quad (3.33)$$

Gas composition downstream of the mixing point is calculated based on streams 11 and 12. The component balances for the mixing points are given below from equations (3.34) to (3.36).

$$\dot{V}_{g,13} * y_{O_2,13} = \dot{V}_{g,11} * y_{O_2,11} + \dot{V}_{g,12} * y_{O_2,12} \tag{3.34}$$

$$\dot{V}_{g,13} * y_{CO_2,13} = \dot{V}_{g,11} * y_{CO_2,11} + \dot{V}_{g,12} * y_{CO_2,12} \tag{3.35}$$

$$\dot{V}_{g,13} * y_{H_2O,13} = \dot{V}_{g,11} * y_{H_2O,11} + \dot{V}_{g,12} * y_{H_2O,12} \tag{3.36}$$

The O_2 balance for ESP and BF is given in equation (3.37) and equation (3.38) below.

$$y_{O_2,FA,23} * \dot{V}_{FA,23} = y_{O_2,14} * \dot{V}_{g,14} - y_{O_2,13} * \dot{V}_{g,13} \tag{3.37}$$

$$y_{O_2,FA,24} * \dot{V}_{FA,24} = y_{O_2,15} * \dot{V}_{g,15} - y_{O_2,14} * \dot{V}_{g,14} \tag{3.38}$$

Gas composition in stream 14 is determined by using the CO_2 and H_2O balances over the BF given in equations (3.39) and (3.40).

$$\dot{V}_{g,15} * y_{CO_2,15} = \dot{V}_{g,14} * y_{CO_2,14} \tag{3.39}$$

$$\dot{V}_{g,15} * y_{H_2O,15} = \dot{V}_{g,14} * y_{H_2O,14} \tag{3.40}$$

$$\dot{V}_{g,15} * y_{O_2,15} = \dot{V}_{g,14} * y_{O_2,14} \tag{3.41}$$

It is assumed that the gas composition remains unchanged in stream 1, 7 and 12.

3.3 Auxiliary relations

To solve the system a set of auxiliary relations is used. These provide extra equations and parameters to improve the accuracy of the model.

3.3.1 Heat losses

For large surface area- and non-insulated equipment such as the mill, coarse separator, and the cyclones the heat loss is estimated. This is done to enhance the accuracy of the model. For

calculating this, the surface temperature is measured using a pyrometer. Ambient temperature is measured and assumed constant. The given heat loss is then calculated using equations (3.42) to (3.44).

$$Q_{loss,AFM} = h_c * A_{AFM} * (T_S - T_A) \tag{3.42}$$

$$Q_{loss,Sep} = h_c * A_{Sep} * (T_S - T_A) \tag{3.43}$$

$$Q_{loss,Cyc} = h_c * A_{Cyc} * (T_S - T_A) \tag{3.44}$$

Heat loss from ducts is neglected since the hot gas ducts are insulated. The duct from AFM to the ESP is not insulated, but heat loss here will not affect the AFM energy balance.

The convective heat transfer coefficient[4] and calculated values are given in Appendix C.

3.3.2 Specific heat capacity

The specific heat capacity is calculated upstream of the AFM, in stream 1, over the AFM system including coarse separator and cyclones, and finally in streams 13 to 15. From the department inlet, stream 1, to the AFM inlet, stream 7, and in the bypass duct, stream 12, the heat capacity is assumed constant due to no false air intrusion and no change in temperature. Equation (3.45) is used in this calculation. The final mixture capacity is calculated using a calculated gas composition, based on CEMS stack values. This is done with equation (3.47).

The AFM heat capacity is an averaged value based on the in- and outlet heat capacity, calculated with equation (3.45). The mixture is calculated using a gas composition based on local measurements performed prior to calculation.

From the mixing point downstream of the AFM and to the stack the heat capacity is assumed constant due to little variation in temperature and gas composition. The mean value is calculated using equation (3.46) based on the composition in the stack.

$$\frac{Cp}{R} = A + BT + CT^2 + DT^{-2} \tag{3.45}$$

$$\frac{\langle Cp \rangle}{R} = A + \frac{B}{2} * (T + T_0) + \frac{C}{3}(T^2 + T_0^2 + T * T_0) + \frac{D}{T * T_0} \tag{3.46}$$

$$C_{p_{Mixture}}^{ig} = \sum y_i * Cp_i \tag{3.47}$$

The heat capacity is calculated for STD and LA production and, due to minor variations in composition and temperature, kept constant for each type produced. Constants used in the calculations are shown in Appendix D[5].

3.3.3 Gas and raw materials ΔT

In the AFM, coarse separator, and cyclones the temperature difference between the raw materials and the gas stream is given a specified value based on measured temperatures. This will remove the need for specifying the temperatures on the solids being separated out in the coarse separator and cyclones and keep the difference consistent with the given gas temperatures.

Then for the extended system with WHRU operating it is assumed that the temperature difference remains the same and by that removing one unknown variable from the system of equations. The ΔT is given from equation (3.48) to (3.51).

$$\Delta T_8 = T_8 - T_{RM8} \tag{3.48}$$

$$\Delta T_9 = T_9 - T_{RM9} \tag{3.49}$$

$$\Delta T_{19} = T_8 - T_{RM19} \tag{3.50}$$

$$\Delta T_{20} = T_{10} - T_{RM20} \tag{3.51}$$

3.3.4 Efficiencies

The efficiencies describe how well particles are separated from the gas stream in the different components of the system. In the coarse separator the efficiency is calculated based on measurements to see the flowrate of materials being separated. For the remaining equipment an efficiency is assumed based on common practice in literature.

$$\eta_{Sep} = \frac{\dot{m}_{RM,19}}{\dot{m}_{RM,8}} \tag{3.52}$$

$$\eta_{Cyc} = \frac{\dot{m}_{RM,20}}{\dot{m}_{RM,9}} \tag{3.53}$$

$$\eta_{ESP} = \frac{\dot{m}_{RM,21}}{\dot{m}_{RM,13}} \tag{3.54}$$

$$\eta_{BF} = \frac{\dot{m}_{RM,22}}{\dot{m}_{RM,14}} \tag{3.55}$$

Efficiencies used in the model is given in Table 3.1.

Table 3.1 Efficiencies

Part	**Efficiency**
Cyclones	90%
ESP	97%
Bag Filter	99%

3.3.5 Heat generated from compression

The increase in temperature over the AFM ID fan is calculated under the assumption of isentropic compression and a fan efficiency of 70%[5].

$$T_2' = T_1 * \left(\frac{p_2}{p_1}\right)^{R/C_p} \tag{3.56}$$

$$T_2 = T_1 + \frac{T_2' - T_1}{\eta_{FAN}} \tag{3.57}$$

3.3.6 Conversion

For conversion between mass and volumetric flow rates equation (3.58) is used. Conversion between standard and actual conditions is done with equation (3.60).

$$\dot{V}_{H_2O,vap} = \frac{R * T_N * \left(w_{H_2O} * \dot{m}_{RM,18}\right)}{MM_{H_2O} * p_N} \tag{3.58}$$

$$\dot{V}_{g,N} = \dot{V}_g * \frac{T_N * p}{T * p_N} \tag{3.59}$$

3.4 Gas composition

Due to intrusion of false air and evaporation of water in the raw materials, the gas composition will be subject to variations throughout the system. This in turn affects the density, heat capacity, and the molecular weight of the gas. To compensate for these variations the gas composition is calculated in all streams based on the values from the stack online analyzer.

Concentrations are calculated based on the following knowledge.

- CO_2 mass flow is constant throughout the system
- Total amount of water added to the system through raw materials
- Sources of false air, and their flow rates are known due to supplementary O_2 measurements over filters and total O_2 balance (3.28).

3.5 Temperatures and condensation

A gas' ability to hold water changes with the temperature, with a decreasing ability with decreasing temperature. So to avoid condensation of water in the ducts the temperature must be kept above the dewpoint. The lowest temperature is seen in the area before and after the ID fan, where it ranges from 55°C to 72°C during current operation, with condensation seen during LA production at temperatures below 52°C. After the mixing point the AFM gas is mixed with hot gas from the preheater or WHRU, such that the temperature increases.

The dewpoint, where relative humidity reaches 100%, is calculated with equation (3.60) where the partial pressure of water is divided by its vapor pressure. Vapor pressure is calculated using the Antoine equation with constants for water in the temperature range from 1°C to 99°C, given in Appendix E. The partial pressure is based on the water content in the flue gas and the pressure. Together these form the equation seen in (3.61).

$$RH = \frac{p_{H_2O}}{VP_{H_2O}} * 100 \tag{3.60}$$

$$RH = \frac{y_{H_2O} * p}{10^{\left(A - \frac{B}{C+T}\right)}} * 100 \tag{3.61}$$

3.6 Extending the model for WHRU calculation

Based on the model describing the current system, for both STD and LA, the new WHRU is incorporated to calculate the new gas streams and temperatures. Post installation of the WHRU the AFM temperature is adjusted by controlling the WHRU-fan speed. This way the hot gas stream from the preheater can be directed and split as needed in the first separation point shown in Figure 2.8. During STD production all gas is directed through the WHRU and

the lowest achievable temperature at the AFM inlet is the recovery unit outlet temperature in stream 5, which is designed to be 170°C. Therefore, during LA production, the temperature must be increased by directing hot gas from the preheater directly to the AFM. By combining stream 2 and 6 the wanted temperature can be achieved through WHRU fan- and ID fan speed control. The following assumptions are made when incorporating the WHRU into the model:

- Raw meal department inlet temperature is raised to 360°C due to shutdown of the GCT.
- Total hot gas flow rate is reduced by 20 000Nm^3/h due to crossover.
- All gas directed through WHRU during STD production.
- Bleed of hot gas, in stream 2, directly to the mill during LA production to ensure sufficient temperature.

The model is extended with an energy balance for the first mixing point, and since the original model mass flow is based on stack online measurements a reduction in gas flow is incorporated to account for the crossover duct. The energy balance is only used when solving for LA production and is given in equation (3.62).

$$\dot{m}_{g,2} * Cp_{g,2} * (T_7 - T_2) = \dot{m}_{g,6} * Cp_{g,6} * (T_6 - T_7) \tag{3.62}$$

New temperature relationships are added to the model as described in equations (3.63) to (3.67).

$$T_1 = T_2 \tag{3.63}$$

$$T_1 = T_3 \tag{3.64}$$

$$T_4 = T_5 \tag{3.65}$$

$$T_5 = T_6 \tag{3.66}$$

$$T_5 = T_{12} \tag{3.67}$$

For STD production with the WHRU in operation the additional temperature relationship (3.68) holds true.

$$T_6 = T_7 \tag{3.68}$$

4 Measurements

Several measurements were done to supplement the calculation with necessary data as well as for validation of the results. These measurements included O_2 and H_2O concentrations in the gas streams, raw material temperatures in and out of the mill system and equipment surface temperatures. All measurements are performed during stable operations for both STD and LA production. Equipment used in measurements are

- Testo 340 flue gas analyzer for O_2 and velocity measurements, equipped with pitot tube and flue gas probe
- Pyrometer for surface temperatures
- Digital thermometer for measuring temperatures in solids

For H_2O a complete description of the equipment is given in chapter 4.2.

4.1 Velocity measurements

Gas velocity is measured at the raw meal department inlet, in the bypass duct and upstream the ESP. These values are used for calculation of flow rates and thereby provide actual flow rates for comparison with calculated flow rates. The flow rates are also used in the calculations to determine the water fraction the raw materials.

The Testo 340 is used with a 2-meter pitot tube and measurements are performed as shown in Figure 4.1. By traversing the cross-sectional area of the duct, variations in the velocity due to the geometry is averaged. This procedure is repeated 2 times at each location, with cleaning of the pitot tube and zeroing of device sensors in between. Obtained values are averaged to provide more reliable data.

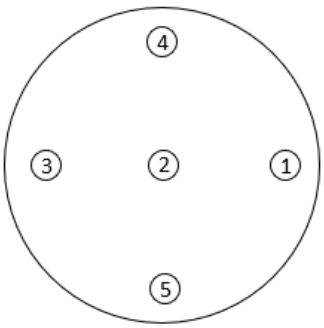

Figure 4.1 Probe locations

Calculation of the gas flow velocity is done using equation (4.1) [6]. A complete table with the differential pressures measured in all locations is found in Appendix F.

$$v_g = \sqrt{\frac{575 * \Delta p * (T + 273.15)}{P_{abs}}} * \alpha \tag{4.1}$$

Ductwork diameters are gathered from technical drawings and the flow rate is calculated before conversion to standard conditions using equation (3.60). Duct diameters is found in Appendix G. Results are given in Table 4.1.

Table 4.1 Velocity measurements

Location	Units	STD	LA
Department inlet velocity $(v_{g,1})$	[m/s]	29.79	31.46
Department inlet flow rate $(\dot{V}_{g,1})$	[Nm^3/h]	163 368	152 728
Bypass-duct velocity $(v_{g,12})$	[m/s]	12.45	13.42
Bypass-duct flow rate $(\dot{V}_{g,12})$	[Nm^3/h]	84 285	80 496
ESP inlet velocity $(v_{g,12})$	[m/s]	34.54	31.01
ESP inlet flow rate $(\dot{V}_{g,13})$	[Nm^3/h]	279 744	244 194

4.2 Moisture measurements

To calculate the moisture fraction in the raw materials, the H_2O concentration is measured up- and downstream of the AFM. This is done by extracting the gas with a heated probe and passing it through a set of bottles immersed in cold water. This causes the water to condense and allow for weighing of the collected water. The gas is extracted at a flow rate of approximately 5 liters per minute over one hour and the accumulated gas volume is measured. The gas temperature into the sampling device is measured every 10 minutes and averaged over the measurement period with equation (4.2) [7].

$$T_{avg} = \frac{1}{n}\sum_{n=1}^{n} T_i \tag{4.2}$$

Then the measured dry gas volume is converted to standard conditions with equation (4.3). The pressure term is ignored due to conditions approximately equal to atmosphere.

$$\dot{V}_{m,ref} = (V_2 - V_1) * \frac{T_N}{T_m} \tag{4.3}$$

The water vapor content, expressed as volume concentration in wet gas is then given by equation (4.4).

$$y_{H_2O} = \frac{\frac{m_{H_2O} * V_{mol}}{MM}}{\frac{m_{H_2O} * V_{mol}}{MM} + V_{m,ref}} \tag{4.4}$$

Measurements are done during STD and LA production to see how the water injection in the GCT, and the raw material water content varies between the types. The results are given in Table 4.2 below.

Table 4.2 Water vapor in streams

Location	**Units**	**STD**	**LA**
Upstream hot gas fan $(y_{H_2O,1})$	[%]	21.59	17.62
Downstream of AFM $(y_{H_2O,11})$	[%]	9.73	11.59

The lowered concentration downstream of the AFM is a result of the false air intrusion at the mill inlet diluting the gas stream. To calculate the water content in the raw materials, equation (3.32) is used to solve for the water vapor flow rate. Further, equation (3.58) is used to calculate the material water fraction w_{H_2O}. Raw material water weight fraction for STD and LA is shown in Table 4.3.

Table 4.3 Water content in raw materials

	Units	**STD**	**LA**
Raw material water fraction $(w_{H_2O,18})$	[%]	0.7	1.8

The higher water fraction in the LA raw material feed corresponds with the increased used of additives, as seen in Table 2.1. The additives are often exposed to rain, and with a finer particle size distribution will hold more water. This holds for Verdal limestone as well as it is stored outdoors.

The calculated weight fractions will be kept constant throughout all simulations.

4.3 Oxygen measurements

Oxygen measurements are done using the Testo 340 flue gas analyzer and a 700mm probe to access the ducts. Probing was done from close to center moving out towards duct wall to ensure measurement consistency. The Testo 340 provides measured values on a dry basis which is converted to wet basis using equation (4.5).

$$y_{O_2,wet} = y_{O_2,dry} * \left(1 - y_{H_2O}\right) \tag{4.5}$$

Under the assumption that false air intrusion is occurring mainly at AFM inlet, and in the filters the O_2 volume fraction is measured up- and downstream of the AFM and both ESP and bag filter. These measurements allow for calculation of the false air intrusion rate in all locations and thereby serves as verification to the model results.

For conversion between dry and wet basis, the measured H_2O content is used for stream 1 and 11, whilst for stream 13 and 14 this value is calculated. Stream 15 is based on CEMS stack value. Stream 13 is calculated using the H_2O component balance for the mixing point downstream of the AFM given in equation (3.36). For calculating the H_2O fraction in stream 14 the gas flow rate must be found. This is done by combining the BF O_2 balance in (3.42), BF H_2O balance in equation (3.40), BF mass balance in (3.6) and the conversion equation given in (4.5). The full procedure and results for each measurement is given in Appendix H.

The final converted wet basis results are given below in Table 4.4.

Table 4.4 Wet basis O_2 measurements

Location	Units	STD	LA
Oxygen fraction upstream AFM $\left(y_{O_2,7}\right)$	[%]	5.16	6.32
Oxygen fraction downstream AFM $\left(y_{O_2,11}\right)$	[%]	13.43	13.69
Oxygen fraction upstream ESP $\left(y_{O_2,13}\right)$	[%]	11.09	11.04
Oxygen fraction upstream bag filter $\left(y_{O_2,14}\right)$	[%]	11.24	11.21

Oxygen fraction downstream bag filter $(y_{O_2,16})$	[%]	11.43	11.52

The results given in Table 4.4 are used for validation of the false air intrusion flow rate calculated in the model, and to determine and set the false air flow rate in the filters. This flow rate is kept constant in the model due to it only being subject to fluctuations if ESP inlet pressure is changed. This flowrate is calculated with the ESP and BF O_2 balances given in equations (3.37) and (3.38), and the mass balances in equations (3.6) and (3.7). Results are given in Table 4.5.

Table 4.5 False air flow rate in filters

Location	Units	STD	LA
ESP ($\dot{V}_{FA,23}$)	[Nm^3/h]	4 193	5 542
BF ($\dot{V}_{FA,24}$)	[Nm^3/h]	5500	8 218

4.4 Mass flow measurements

The efficiency of the coarse separator, and its ability to separate solids from the gas stream will affect the AFM energy balance by shifting the mass flow between the separator and cyclone, thereby changing the energy requirement due to temperature differences.

To calculate the coarse separator efficiency the flow rate of materials being separated is measured. This is done by measuring the conveyor belt speed downstream of the coarse separator and weighing the materials covering 1 meter of the belt. Prior to this the RM bypass belt, shown in Figure 2.1, is stopped and by that isolating the material stream from the separator. For calculating the mass flow rate out of the separator equation (4.6) is used.

$$w_{RM,Con} * v_{Con} = \dot{m}_{RM,19} \tag{4.6}$$

Using equation (3.16), with the calculated water fraction given in Table 4.3, the mass flow rate into the separator is calculated and the efficiency is found with equation (3.52). Basis for the calculation and efficiency are shown in Table 4.6. The efficiency is only calculated during STD production. Minor fluctuations might occur with different materials and gas velocities.

Table 4.6 Calculation of coarse separator efficiency

Location	Units	STD
RM feed rate	[kg/h]	260 000
Bypass flow rate	[kg/h]	60 000
AFM feed rate ($m_{RM,18}$)	[kg/h]	200 000
Conveyor belt material load	[kg/m]	30.923
Belt speed	[m/s]	1.123
Coarse separator out ($\dot{m}_{RM,19}$)	[kg/h]	125 015
Efficiency η_{Sep}	[%]	62.5

4.5 Temperature measurements

4.5.1 ΔT estimation

To determine the temperatures of the raw materials going in and out of the system several measurements are done. Material feed to the mill is measured using a pyrometer along with the material stream going out of the coarse separator. Materials separated in the cyclones are measured with a wired digital thermometer. The results are given in Table 4.7.

Table 4.7 Temperature measurements

Location	Units	STD	LA
Raw material feed to mill $(\dot{m}_{RM,18})$	[°C]	11.0	11.0
Solids out of coarse separator $(\dot{m}_{RM,19})$	[°C]	55.0	50.2
Raw meal out of cyclones $(\dot{m}_{RM,20})$	[°C]	57.3	52.0
Ambient air (T_{FA})	[°C]	20.0	20.0

These temperatures are used for setting the ΔT values in the model by rearranging the equations given from equation (3.48) to (3.51) and implementing them in the AFM system energy balance. Running iterations with the system and changing the ΔT value the RM outlet

temperatures in the coarse separator and cyclones can be compared to the measured values. When the calculated and measured temperatures match the ΔT value is set and used for all STD and LA models, and by that removing one unknown variable when using the model for the WHRU calculations.

See Appendix I for the implementation of ΔT equations in the energy balances. The resulting ΔT's are listed in Table 4.8.

Table 4.8 ΔT values

Location	**Units**	**STD**	**LA**
AFM (T_{RM8})	[°C]	25	20
Coarse separator out (T_{RM19})	[°C]	16	11
Downstream coarse separator (T_{RM9})	[°C]	11	4
Cyclones out (T_{RM20})	[°C]	10	3

4.5.2 Hot gas temperature measurement for validation purposes

To ensure the reliability of the temperature measurements provided by PxData some of the measurements are done manually. Point temperatures are measured as shown in Figure 4.1. Uniform values are measured at the department inlet and in the bypass duct, but upstream the ESP, in stream 13, some stratification is seen. This is due to the gas flow from the bypass duct and AFM ID fan not mixing properly. The results are given in Table 4.9

Table 4.9 Hot gas temperatures

Location	**Units**	**STD**	**LA**
Department inlet temperature (T_1)	[°C]	185.10	245.10
Bypass-duct temperature (T_{12})	[°C]	184.90	245.00
ESP inlet temperature (T_{13})	[°C]	108.14	119.02

5 Results

Several process parameters used to solve the model are based on online measurements from the plant control system, with data accessible from the online data platform PxData. These parameters make up the foundation on which the model is based and solved. Measured data from chapter 4 is used to validate model results and for calculating constant values in the model. In Table 5.1 the different cases that are to be investigated are shown.

Table 5.1 Different cases solved in model

NR	Case	Chapter
1	STD production model results	5.1.4
2	LA production model results	5.1.5
3	STD WHRU model results	5.2.4
4	LA WHRU model results	5.2.5
5	STD production with WHRU and no false air	5.3.1
6	LA production with WHRU and no false air	5.3.2
7	Reduced false air for STD and LA	5.3.3
8	H_2O concentration and temperature considerations	5.4

By solving these cases the influence the WHRU and false air have on the system can be assessed, along with the reduction in flue gas H_2O content. The operational constraints will be considered based on the data provided by the model.

5.1 STD and LA operation today

5.1.1 Process data

Data gathered from the process control system includes gas composition, temperature, and flow rate in the stack as well as O_2 level and temperature from the preheater. The temperature up- and downstream of the AFM system is used along with the raw material feed to the mill. In Table 5.2 these values are presented for both STD and LA production, and the listed values are collected during stable operation to ensure their representativity.

Table 5.2 Online process data

Parameter	Units	STD	LA
Raw meal department inlet O_2 ($y_{O_2,1}$)[2]	[%]	4.51	6.10
Stack O_2 ($y_{O_2,15}$)	[%]	11.43	12.00
H_2O in gas going to stack ($y_{H_2O,15}$)	[%]	12.67	12.26
Gas temperature into raw meal department (T_1)	[°C]	185	245
AFM inlet gas temperature (T_7)	[°C]	185	245
ID fan gas temperature (T_{10})	[°C]	67	56
AFM inlet pressure	[mbar]	-1.1	-1.1
ESP inlet pressure	[mbar]	-7.5	-6.0
Gas flow rate going to stack ($\dot{V}_{g,15}$)	[Nm^3/h]	282 534	259 543
Raw material feed rate to mill ($\dot{m}_{RM,18}$)[3]	[Ton/h]	160	238

5.1.2 Heat capacity considerations

Due to the temperature differences along the system, and the different temperature requirements for STD and LA, the heat capacity is taken into consideration in the model. Values given in Table 5.3 are calculated as described in chapter 3.3.2.

Table 5.3 Heat capacities used in original model

Location	Units	STD	LA
Hot gas upstream AFM system	[kJ/kgK]	1.219	1.209
AFM Gas	[kJ/kgK]	1.119	1.146

[2] Manual measurement for STD

[3] PxData value minus 60t/h for STD and 10t/h for LA

AFM Solids	[kJ/kgK]	0.78	0.78
Downstream mixing point	[kJ/kgK]	1.101	1.1245

5.1.3 Solving the model

The model is programmed and solved in Maple 2021. All mass, energy, and component balances with auxiliary relations are specified, along with the parameters given in Table 5.2. Additional raw material H_2O fractions, and temperatures known from measurements are used to calculate constants used in the model.

The model first calculates the inlet gas flow using the total mass and O_2 balance. When this value is established the AFM inlet false air intrusion is calculated based on the difference between the in- and outlet flow rate of the system, minus the false air in the ESP and BF. ESP and BF flow rates are known from O_2 measurements and are established separately.

Raw materials and solid streams are calculated to define the material flow within the coarse separator and cyclone. This is done by applying the efficiencies given in Table 3.1 and the calculated coarse separator efficiency. Water vapor added to the system through evaporation of water in raw materials is calculated based on the H_2O fraction the raw materials.

Then the model calculates the hot gas flow rate requirement at the inlet to reach the specified AFM outlet temperature. This is achieved by rearranging the coarse separator and cyclones energy balances as functions of the gas temperature. These equations are then used in the AFM energy balance, and the hot gas mass flow in stream 7 is solved for. This is based on the AFM in- and outlet temperatures. When the needed gas flow in stream 7 is established the bypass duct flow rate is calculated, and by that, defining the system gas flow rates.

Gas temperature upstream of the ESP is calculated using the mixing point energy balance, along with the temperatures downstream the ESP and in the stack with the ESP and BF energy balances.

Lastly the model solves the O_{2}-, H_2O- and CO_2-component balances to define the streams composition throughout the system.

The model is solved in its entirety in Appendix J to show the procedure for STD production. Process parameters are gathered and plotted in Appendix K for STD and LA for the periods where the measurements were performed. The model represents the production in these time periods.

5.1.4 STD production model results

To validate the model, all input parameters are collected in the same period as the measurements are performed. The resulting gas flow rates for STD production are shown in Figure 5.1. The model shows good correspondence with the measured values but underestimates the false air intrusion at the AFM inlet. The calculated hot gas flow rate in the AFM matches the measured value, but with an increase in false air to the measured value, a further increase in hot gas would be needed.

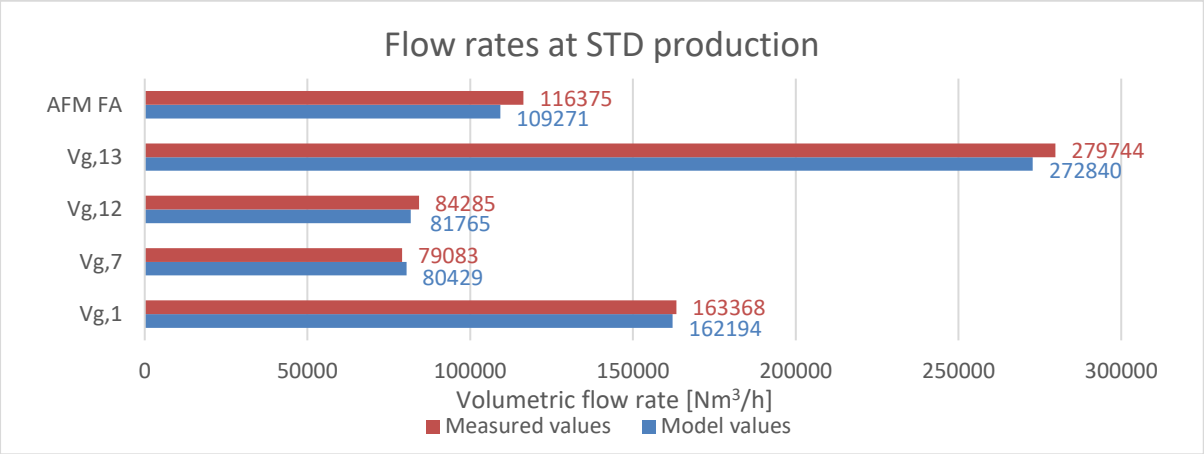

Figure 5.1 Flow rates at STD production

Gas temperatures are calculated at the AFM- and coarse separator outlet, downstream the mixing point, downstream of the ESP and eventually in the stack. AFM and separator outlet temperatures are not accessible for measurements, such that these are not verified. The temperature downstream of the mixing point is available as an online measurement, but due to stratification of the gas stream this temperature may vary with gas velocities and bypass duct temperatures. So for comparison, the temperature acquired from measurements given in Table 4.9 is used. Calculated temperatures for STD production are shown in Figure 5.2.

For STD production the relative humidity is calculated, using equation (3.61), to be 35% and no condensation is expected to occur.

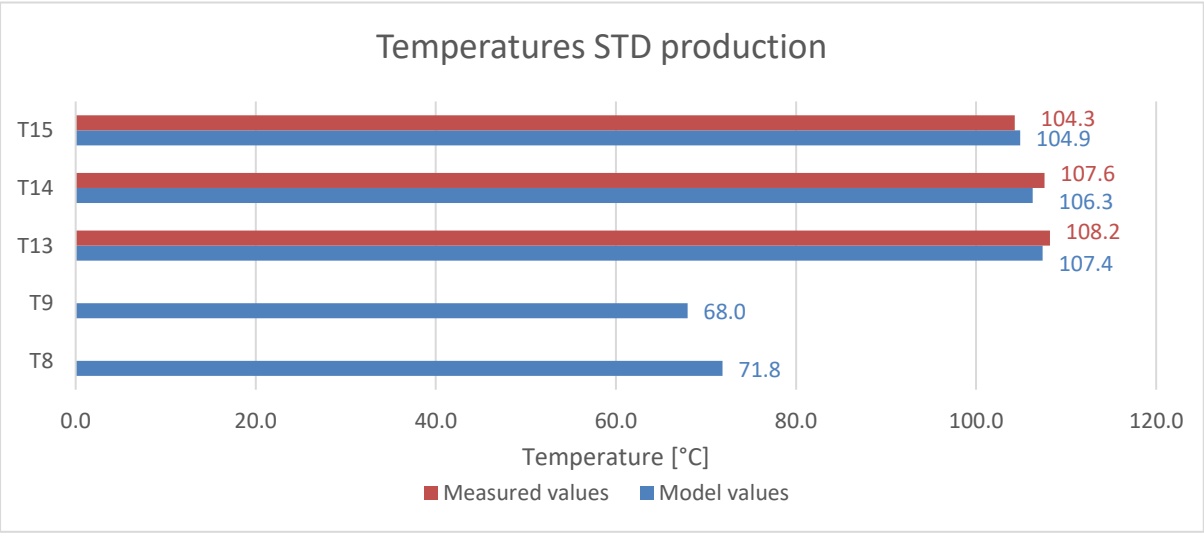

Figure 5.2 Temperatures STD

Based on the ΔT's set for the system the temperature profile in the AFM, coarse separator, and cyclones is shown in Figure 5.3. A small increase in temperature from the separator outlet to cyclone inlet is expected, as well as the final temperature rise in particles not separated in the cyclones. Only the smallest particles are entrained by the gas stream out the cyclones, thus the assumption of thermal equilibrium.

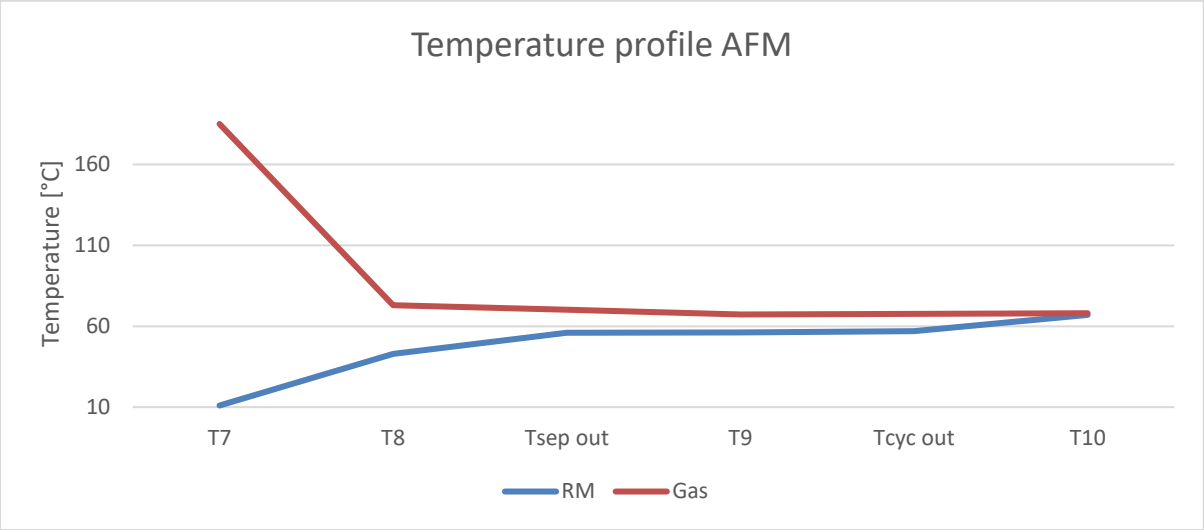

Figure 5.3 STD AFM temperature profile

The gas composition is calculated throughout the system and varies with the false air intrusion and evaporation of water from the raw materials. For streams ranging from 1 to 7, and 12, the composition remains unchanged due to the assumption of no false air upstream the AFM, and no water added to the system.

During STD production stream 7 has a high water load due to the increased water injection rate in the GCT to reach the low temperature needed. In the AFM, due to high false air intrusion, this is concentration is diluted before it increases again when the gas is mixed with the bypassed gas. The O_2 concentration changes correspondingly, with the highest concentration downstream the AFM. For the O_2 concentration at the model inlet a manually measured value is used for STD production and not the online value from PxData. This was done due to a deviance between the measurements that indicated a too low O_2 concentration downstream of ESP3. Using the online value in the model would have increased the false air with >13 000Nm^3/h and reduced the AFM inlet temperature with 12°C. The temperature was not affected, indicating no considerable false air in the duct between ESP3 and the raw meal department, justifying the use of the manual measured value. See Appendix L for calculation.

Minor O_2 changes are seen in the filters due to the predetermined false air intrusion. The gas composition profile for STD production is shown in Figure 5.4.

The CEMS analyzation values for O_2 and H_2O is listed with stream 15 as they are the same value. For the sake of comparison, point measurements of O_2 and H_2O is plotted. These show good correspondence with the calculated values.

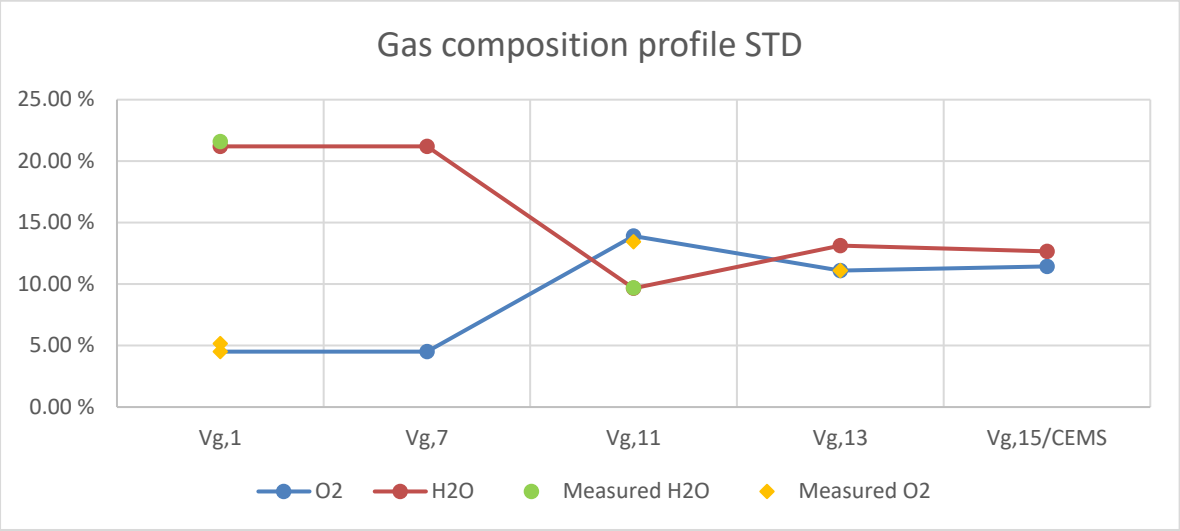

Figure 5.4 Gas composition profile STD

The complete flowsheet for STD production with calculated values is given in Appendix M.

5.1.5 LA production model results

For LA production the model slightly overestimates the false air at the AFM inlet. A false air flow rate corresponding to the measured value would reduce the hot gas flow in the AFM and increase the flow rate in stream 12. This indicates that the O_2 input in the model is slightly erroneous as the reduced energy requirement would shift hot gas from stream 7 to stream 12, and thereby correspond to the measurements. But overall the model achieves comparable results. Results for LA is shown in Figure 5.5.

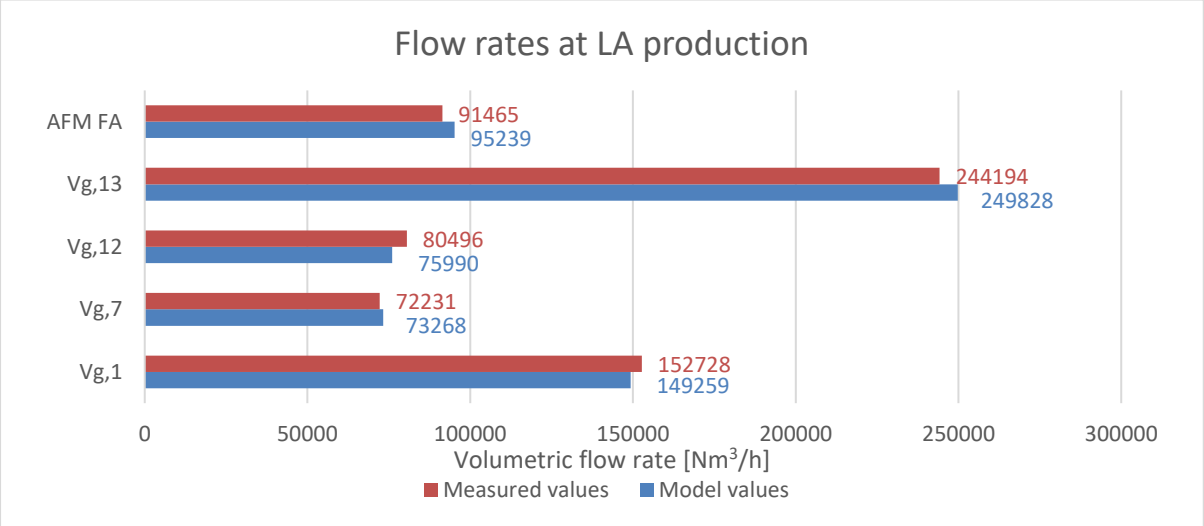

Figure 5.5 Flow rates at LA production

The calculated temperatures are compared to the measured temperatures in Figure 5.6. Measured values in stream 13 and 14 are based on manual measurements. For stream 15 the online temperature is used.

With an AFM outlet temperature of 56°C a relative humidity of 71% is calculated. This is closer to the saturation point relative to during STD production, but no condensation should occur.

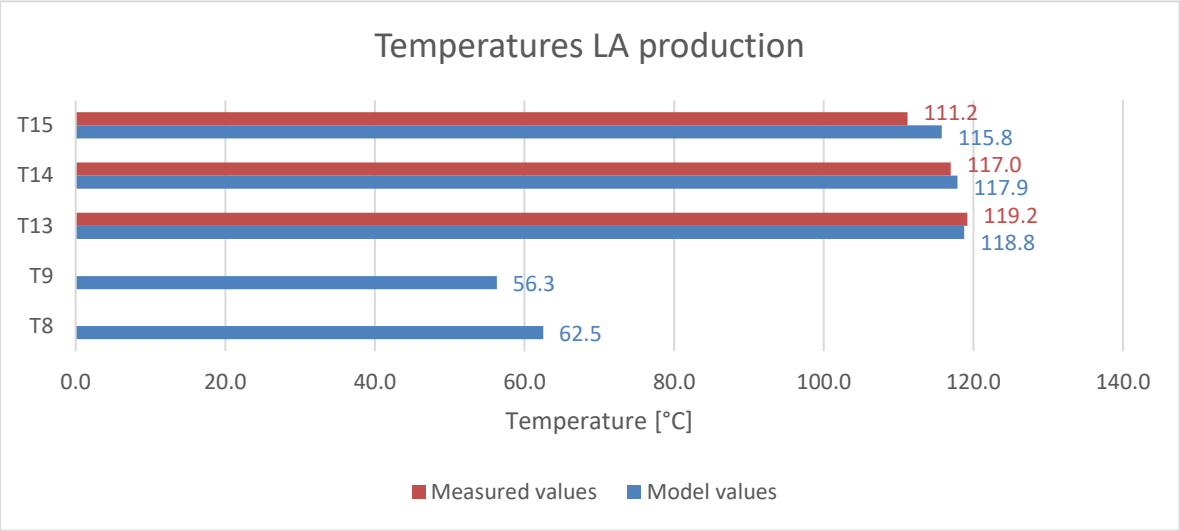

Figure 5.6 Temperatures LA

During LA production, with the increased temperature at the inlet, the water load is lessened due to the reduced water injection rate in the GCT. Still, an increase in the H_2O concentration, relative to STD, is seen downstream of the AFM. This corresponds well with the higher H_2O fraction and feed rate of the materials used in LA production. For the O_2 concentration in stream 1, the online measurement is used, and this corresponds well with the manually measured value.

The increased H_2O concentration downstream of the AFM indicated by a point measurement is likely due a higher raw material feed rate at the time of measurement.

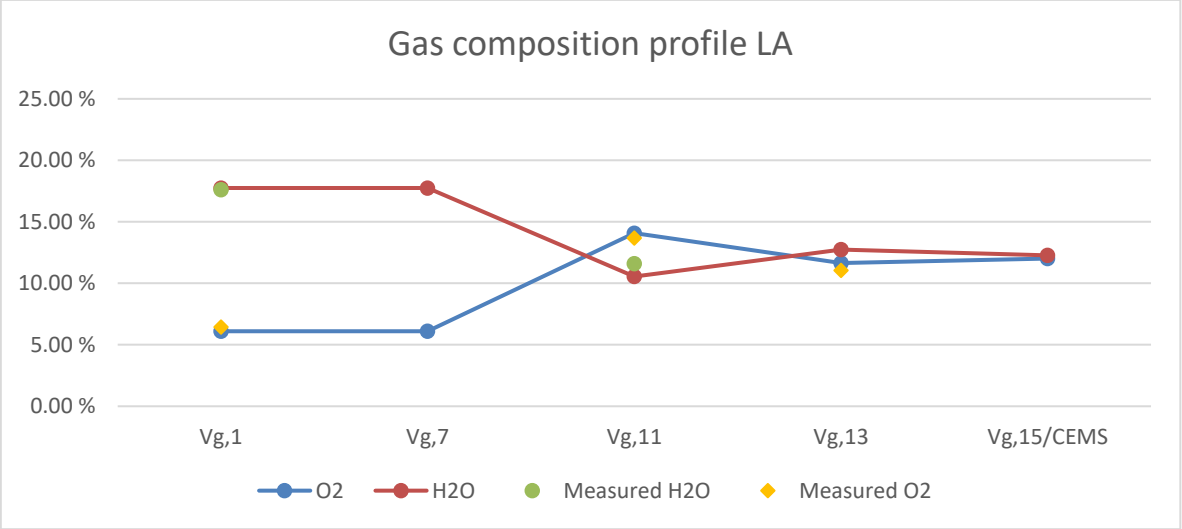

Figure 5.7 Gas composition profile LA

For LA production the calculated values are given in Appendix N.

5.2 STD and LA operation with WHRU

The original model is extended as described in chapter 3.6 and used to solve the new system. For STD, with the new inlet temperatures, the system is solved based on the absolute volumetric flow rate in stream 8 in the original model, and the AFM outlet temperature is reduced accordingly. This is to preserve the production capacity.

5.2.1 Process data

Most of the process data used in the original system are reused in the WHRU system, except for inlet temperature and H_2O concentration. Altered values are shown in Table 5.4.

Table 5.4 WHRU mode parameters

Parameter	Units	STD	LA
Raw meal department inlet temperature (T_1)	[°C]	360	360
AFM inlet temperature (T_7)	[°C]	170	245
H_2O concentration at inlet ($y_{H_2O,7}$)[3]	[%]	9.0	9.0

5.2.2 Heat capacities

With the shutdown of the GCT there will be a reduction in H_2O content in the gas. The composition used in the calculations corresponds to values obtained in earlier measurements[3], where the H_2O content level is 9%. This change in composition along with the new temperatures will change the specific heat capacity of the gas. New values are given in Table 5.5.

Table 5.5 Heat capacities WHRU model

Location	Units	STD WHRU	LA WHRU
Hot gas upstream AFM system	[kJ/kgK]	1.168	1.168
AFM Gas	[kJ/kgK]	1.109	1.130
AFM Solids	[kJ/kgK]	0.84	0.84
Downstream mixing point	[kJ/kgK]	1.066	1.065

5.2.3 WHRU solving

For the WHRU model the AFM balance remains unchanged and the absolute volumetric flow rate in stream 8 should be maintained to keep the current production rate. Since the flow is kept constant the velocity will remain unchanged, and by that ensuring equal carry-over of materials to the coarse separator. The ΔT's remain constant from the original models, but for STD the outlet temperature will change due to the reduced inlet temperature. This temperature is found by iterating the model until the flow rate matches the original flow rate.

For LA production the AFM calculation remains unchanged for the WHRU model due to the inlet temperature being the same. Outlet temperature is adjusted for minor variations to match the absolute gas flow in stream 8 in the original LA model.

5.2.4 STD WHRU model results

The total gas flow rate is lowered with 20 000Nm^3/h due to the crossover installation upstream of the department. Then all the hot gas is passed through the WHRU to recover the available waste heat. In the second separation point the required gas is drawn to the AFM while the remaining gas passes through the bypass duct. The calculated WHRU flow rates are given, along with the calculated values from the original model, in Figure 5.8.

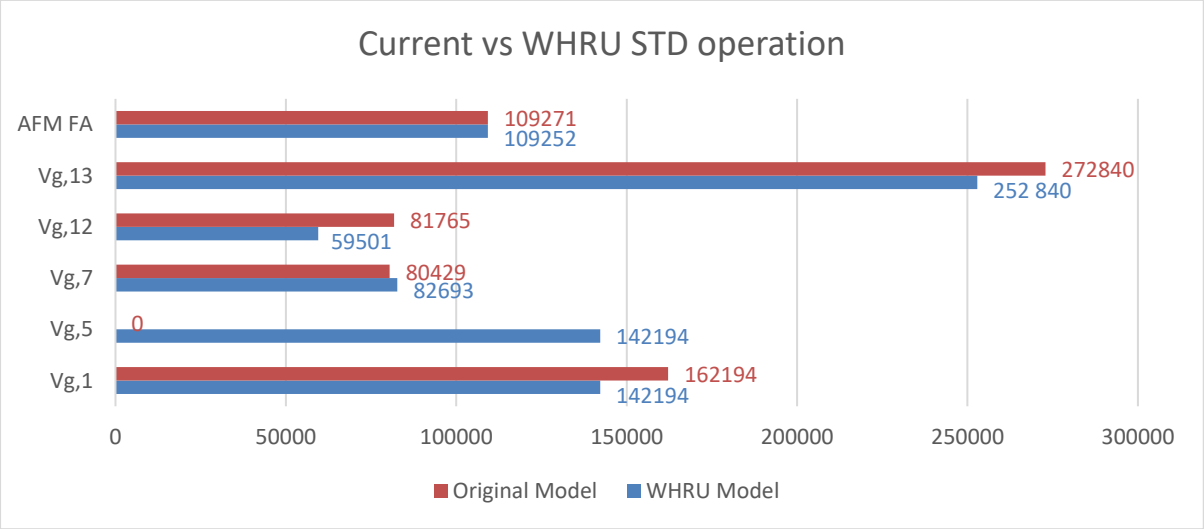

Figure 5.8 STD WHRU flow rates

The absolute flow rate through the AFM is maintained by lowering the outlet temperature to 63.2°C. This keeps the system well above the dew point, with a relative humidity of 42%, and no condensation is expected to occur.

The reduced H_2O concentration in the inlet gas stream reduces the AFM outlet concentration to 4.57%, from 9.66% in the original model. This will allow for a further reduction in temperature based on a lowered saturation point. This will be investigated in a separate case.

Flowsheet with calculated values for STD WHRU is found in Appendix O.

5.2.5 LA WHRU model results

During LA production the AFM inlet temperature can be controlled freely over the temperature range in use today, such that the production should not be affected. The flow rate through the mill is unchanged, but the lowered total flow rate will reduce the bypass-duct flow rate. In turn this, along with a lowered bypass temperature, will reduce the stack temperature from 118 to 88°C, while the lowest temperature is found upstream of the ID fan at 55.3°C. This is 0.3°C above the original LA model.

This increase in inlet temperature is due to changes in gas composition, and the resulting lowered specific heat capacity. By increasing the temperature with 0.3°C the absolute gas flow rate in stream 8 is constant and the production capacity is maintained. Flow rates throughout the system is shown in Figure 5.9.

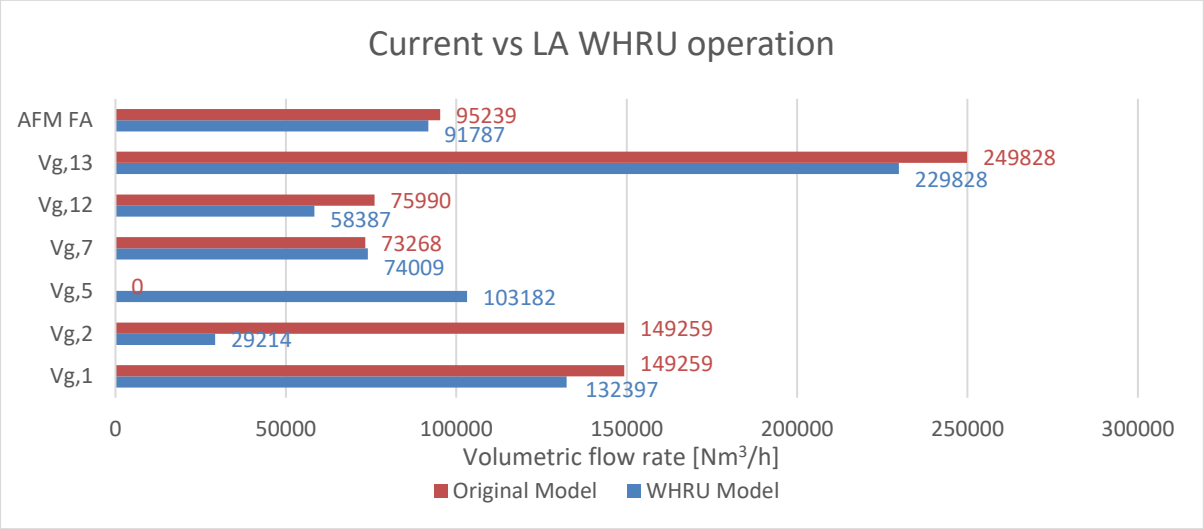

Figure 5.9 LA WHRU flow rates

The H_2O concentration is increased downstream of mill during LA production, relative to STD production. This increase is a direct result of the increased water content in the raw material composition used in LA production. The H_2O profile shown in Figure 5.10 illustrates the difference between H_2O content during STD and LA production.

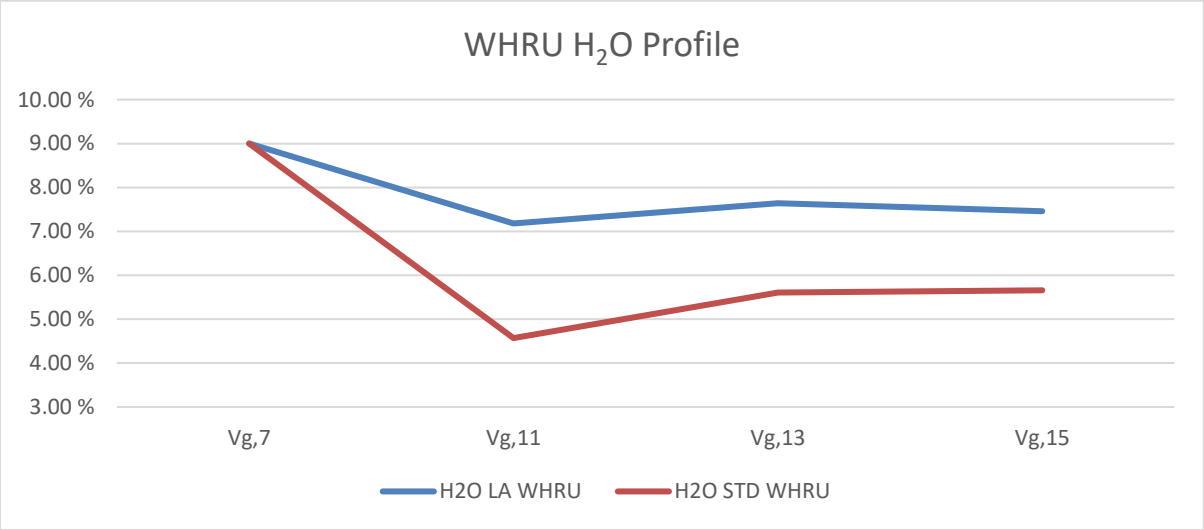

Figure 5.10 WHRU operation H_2O profile

For LA with WHRU in operation the calculated values are given in Appendix P.

5.3 Solving system with changes in false air intrusion

False air intrusion at the mill inlet during WHRU operation accounts for 52 to 56% of the total flow rate through the ID fan. This high flow rate has the following consequences for the AFM system:

- It increases the energy requirements by heating up the ambient air
- Adds to the total flow rate and thereby increases velocity, thus maintaining the production capacity if sufficient heat is available
- Dilutes the H_2O fraction at the AFM outlet and lowers the saturation temperature

From that it is seen that false air intrusion provides sufficient gas velocity for carry-over of materials and increases the energy consumption at the same time. By sealing of the mill inlet and removing the biggest source of false air, the operability and operational parameters would change, relative to the present situation. The gas composition would remain constant except for an increased H_2O fraction in the AFM outlet gas. Secondly the energy requirement would decrease, and a rise in outlet temperature would occur if the present inlet temperatures were to be used. But the most critical point would be the total gas flow rate through the AFM, that must be kept constant, such that any reduction in false air must be replaced with hot gas. In turn this will lead to a sharp increase in temperatures.

To implement this change in the model the O_2 concentration in the stack is lowered to match the department inlet concentration, and stack gas flow is reduced correspondingly. This way the total O_2 balance given in equation (3.28) provides a zero false air gain to the model, and the false air term in the AFM energy balance (3.20) zeroes out. Therefore, the hot gas flow rate into the AFM is reduced as an effect of the reduced energy requirement. In turn this will reduce the carry-over of material and negatively affect the production capacity.

So, to maintain the gas flow rate similar to the models including false air, the absolute flow rate in stream 8 must be kept constant. This is achieved by further increasing the hot gas flow rate in stream 7.

5.3.1 STD production with WHRU and no false air

From the WHRU model with false air the absolute flow rate in stream 8 is 240 970m^3/h. To reach this flow rate the hot gas flow rate in stream 7 must be increased from 82 693Nm^3/h to 166 575Nm^3/h, which supersedes the available gas at the department inlet. With the total deficit being 24 381Nm^3/h.

This increase in hot gas flow rate will cause the AFM outlet temperatures, for both gas and solids, to increase significantly. In Figure 5.11 the resulting temperatures are given.

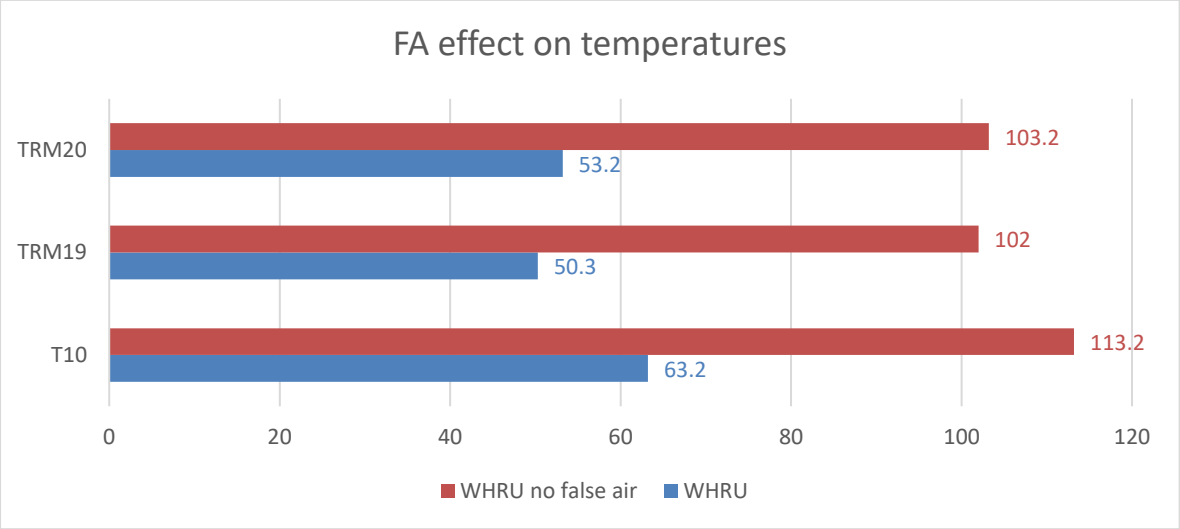

Figure 5.11 Temperatures without FA during STD production

5.3.2 LA production with WHRU and no false air

As with STD production, the required hot gas flow through the mill for LA production is higher than the available amount at the department inlet. The available gas deficit for LA is 23 209Nm^3/h. This is with heat recovery of all the gas and an AFM inlet temperature of 170°C.

Temperatures increase for both gas and solids, but the increase is slightly less than for STD production. The results are given in Figure 5.12.

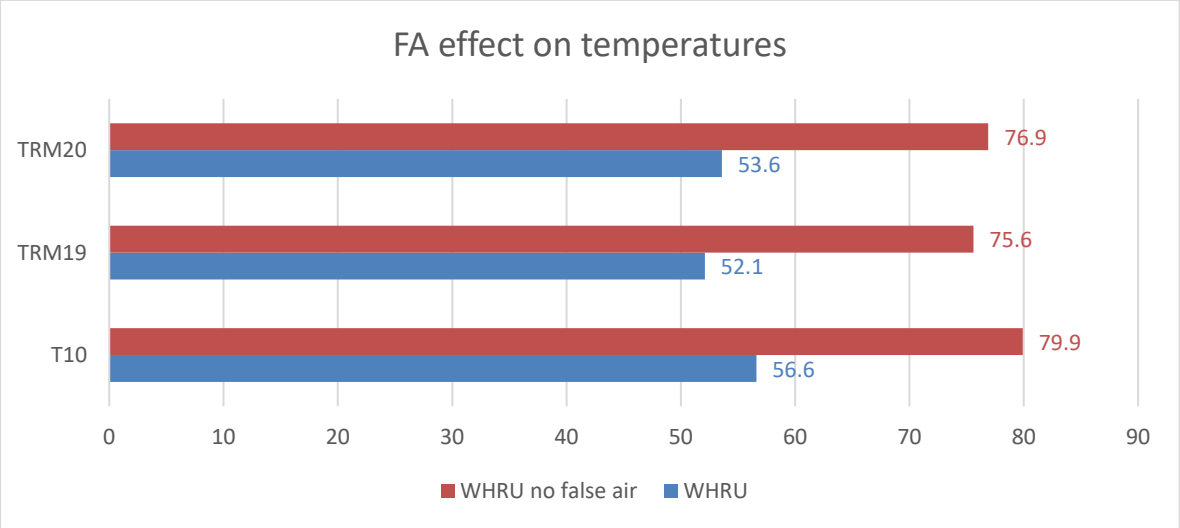

Figure 5.12 Temperatures without FA during LA production

5.3.3 Reduced false air for STD and LA

A third option is to partially seal of the AFM inlet to reduce the false air intake, but not remove it in its entirety, which would be a more realistic option. This allows for additional heat recovery during LA production, but for STD production would only cause a rise in temperatures.

To see how the system changes, the false air is reduced to a level where the required hot gas flow through the AFM matches the available hot gas at the department inlet. This way, all hot gas can be used for heat recovery, and thus an AFM inlet temperature of 170°C is used. With this inlet temperature, the outlet temperature changes to 67.2°C for LA production and the absolute gas flow in stream 8 is maintained.

Since all the gas is used for heat recovery an additional 2.66MW can recovered relative to the original high temperature WHRU model. The basis for this calculation is the increased mass flow through the WHRU, from 135 959 to 179 018kg/h.

Repeating this exercise for STD production will not provide any further heat recovery since all the hot gas already has been utilized. The consequence is an increase in the temperature downstream of the mill to 96.5°C with the resulting increase in solids temperatures as given in Figure 5.14. New flow rates in the system are shown in Figure 5.13.

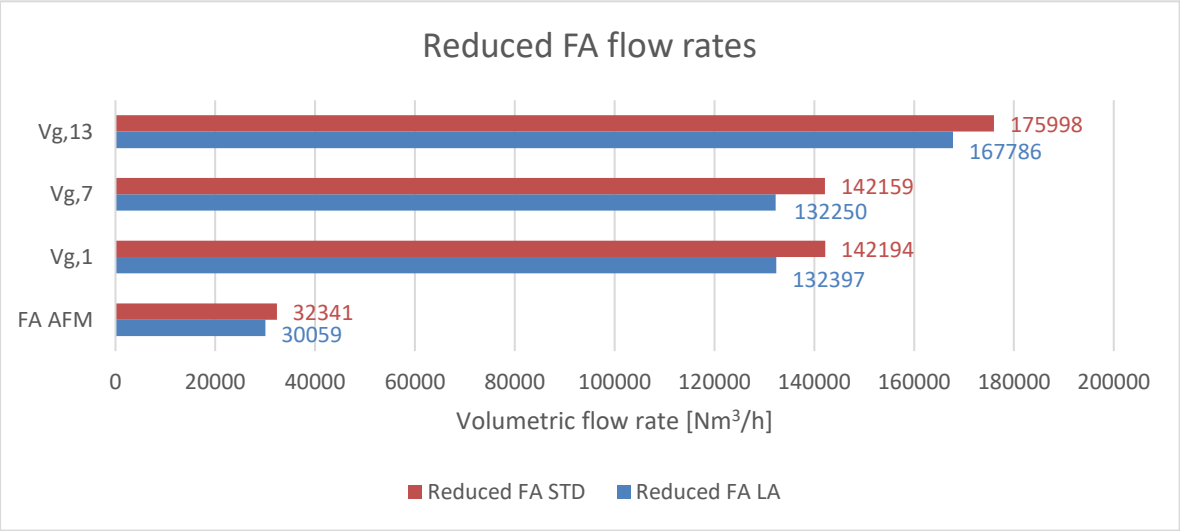

Figure 5.13 Reduced FA volumetric flow rates in STD and LA

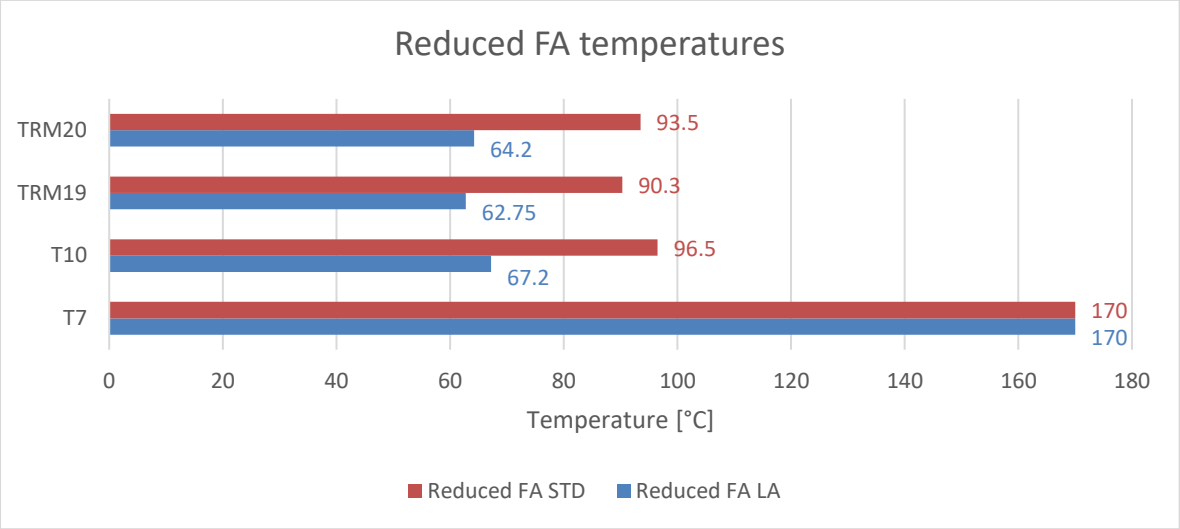

Figure 5.14 Reduced FA temperatures in STD and LA

Flowsheets illustrating the new values for reduced false air intrusion are given in Appendix Q and R for STD and LA, respectively.

5.4 H_2O concentration and temperature considerations

During operation of the WHRU the H_2O load in the gas entering the department is strongly reduced. This will lower the H_2O concentration in the coldest part of the process, and thereby lower the saturation temperature. This in turn can increase the amount of available heat for recovery. Anyhow, this only holds for LA production since STD production already utilizes all available heat. During LA production a reduced temperature will allow for more gas being directed through the WHRU, hence increase the heat recovered.

To determine the lowest acceptable temperature at the AFM outlet, the saturation temperature is calculated for the present situation and compared with the lowest acceptable value based on experience. This is the temperature where plant personnel experience condensation downstream of the AFM. Based on this difference, an ΔT_{RH} is set for use when calculating the new outlet temperature.

Table 5.6 ΔT for saturation temperature

	Units	**STD**	**LA**
Lowest outlet temperature	[°C]	50	52
Relative humidity	[%]	72	82
Today's saturation temperature	[°C]	45	48
ΔT_{RH}	[°C]	5	4

Calculated saturation temperatures, based on H_2O concentration in the gas, are shown in Table 5.7

Table 5.7 Saturation temperatures

System	Units	STD WHRU	LA WHRU
Saturation temperature WHRU	[°C]	31.6	39.9
New outlet temperature	[°C]	36.6	43.9

As seen in Table 5.7 the outlet temperature can be reduced to 43.9°C during LA production, based on the H_2O content in the gas. To maintain the production capacity with this reduced temperature the absolute flow in stream 8 must remain unchanged, and thereby ensuring the same velocity at the AFM outlet. A direct consequence of this will be more hot gas available for heat recovery in the WHRU since less hot gas is passed straight to the AFM in stream 2. Based on the calculated saturation temperature, including the ΔT_{RH}, the new inlet temperature is found by iterating the model until the absolute flow rate in stream 8 matches the flow rate in the high temperature LA WHRU model.

The new inlet temperature is 183.5°C which allows for almost all gas to pass through the WHRU for heat recovery. This will reduce the hot gas mass flow rate in stream 2 and increase the mass flow through the WHRU from 135 959 to 167 100/h thus generate an additional 1.92MW of heat.

A complete flowsheet with all calculated values is given in Appendix S.

6 Discussion

6.1 Model validity

The aim was to develop a model that described the process accurately, and by that having a model to describe the extended system. Several measurements were taken to both supply the model with data and provide data for comparing of results.

6.1.1 Assumptions in the model

Several assumptions were made in the model to simplify the calculation, as seen in chapter 3.1. Among them was the assumption of constant efficiencies for the coarse separator and cyclones, which may vary with gas velocity and particle size distribution. A consequence of this would be a slight shift in the energy balance for the AFM system as more or less materials are being separated out in each component. These small variations were assumed to have negligible effect on the system.

For the false air intrusion it was assumed that it only occurred in the AFM, ESP and BF, with the rate in the filters being constant, only differentiated between the STD and LA models. This holds up if the pressure upstream of the ESP are kept constant, but small variations occur, typically in the range of -5 to -7.5mbar. The O_2 concentration is measured during STD and LA production, with the pressures specified in Table 5.2, and intrusion rates are calculated based on the online stack flow measurement. Changing these pressures will change the false air flow rate but variations should be small compared to the AFM inlet intrusion.

The BF differential pressure should also be included as a source of error in the constant false air flow rates, as a higher differential pressure could increase the false air intrusion at the low-pressure side. Anyhow, these variations will have minor effect on the system upstream.

Thirdly the pressure is assumed to be constant at 1atm throughout the model, despite small pressure gradients. Due to pressures close to atmosphere this assumption should be reasonable.

6.1.2 Validity of measurements

With all the measurements done to supplement this report comes new possible sources of errors and uncertainties. In most cases manually measured values are compared with online values and checked for similarities, but measurements done to supplement the model with data lack these online values. For the H_2O content, this measurement was performed 1 time for each location with the following risk of erroneous results due disturbances in the process. A second measurement would improve the accuracy and validity, but as the raw materials H_2O content changes, the obtained values would only be valid for that specific batch. Still, the calculated H_2O fraction in the raw materials greatly affects the AFM energy balance so any major deviances will cause an under- or overestimation of the required gas flow at the AFM inlet.

In the model the H_2O input is based on data from CEMS and then back calculated to the department inlet where the measured value is compared with the calculated value. Good correspondence between these values indicates valid measurement results.

For the velocity measurements, values from which the volumetric flow rate is calculated, are equally sensitive to disturbances in the process. To enhance the reliability of these measurements they were performed as shown in Figure 4.1 with two separate readings for each position. According to the centroidal axis method given in DIN EN 12599[8] more points is preferrable to provide more reliable results, but this was somewhat restricted with only one access point in the ducts. Validation of the results was done through comparison with the flow rates calculated in the model, which is based on the stack flow analyzer and obtained O_2 values.

The gas temperature measurements were performed in the same manner as the velocity measurements, probing in 5 points traversing the duct. This provided adjustments for online measurements deviating from the measured temperature. Specifically the temperature upstream of the ESP show an increasing offset with increasing flow rate in the bypass duct, due to stratification of the gas. The measured value corresponded well with the calculated value.

6.1.3 AFM energy balance

The heart of the calculation is the AFM energy balance calculating the needed hot gas mass flow at the mill inlet. These equations, (3.20) to (3.22), rely on inputs that are subject to changes between production types, including heat loss to the surroundings, raw material composition, ΔT's in the AFM system, and variations induced by changes in gas composition. Although minor impacts on the system are expected for each variable the combined effect from all of them may be more of significance. Therefore, the values used in this model are rooted in measurements and calculations during stable operation of the system thus should be valid.

For simplicity the specific heat capacity is kept constant throughout the AFM system, including the coarse separator and cyclones. This value will change due temperature and false air, but the mean value used should only induce minor errors. This also holds for the raw materials, where the specific heat for only limestone is considered,

6.1.4 Consideration of other AFM parameters

One aspect that is not considered in the model, and that would benefit from further work, is the relationship between the degree of filling in the AFM, raw material residence time and the gas flow. A reduced filling induces a lower resistance in AFM; thus an increased gas flow rate is seen. Further the increased flow rate reduces the AFM inlet static pressure, which in turn increases the false air flow rate. An increased flow rate brings forward a higher velocity thus a higher production capacity would be expected if the grinding efficiency is maintained with the reduced filling.

This could potentially alter the raw material residence time and outlet temperatures significantly and thereby change the AFM energy requirement. Similarly changes in the raw

material composition, with differences in the materials grindability, will impact the residence time in the AFM, which in turn will affect the raw material feed rate and outlet temperatures.

These considerations are not included in the model and how changes in AFM filling will affect the system, relative to the model, is not identified.

6.2 Overall considerations

6.2.1 False air today and how will this change

False air is a major fraction of the total gas flow through the ID fan, ranging from 52-56% in this work, and thus is an important contributor to gas velocity and carry-over of materials to the coarse separator. By reducing or removing this the hot gas flow rate will have to be increased to compensate for the reduced flow to avoid a reduction in production capacity. Results provided by the model in this work indicate that sealing of the inlet will be undesirable due to the increased outlet temperatures, increasing with the extent to how much false air is replaced by hot gas. Values calculated in these cases are for WHRU operation and not for the present system where the temperatures would increase even further due to a higher AFM inlet temperature. Further a complete sealing of the inlet will induce a gas deficit to the system since the flow rate requirement surpasses available gas.

Partially sealing of the false air is more promising, with the possibility for more heat recovery during LA production, with only slightly increased temperatures. This possibility does not apply for STD production since no additional heat can be recovered and the reduced energy requirement will precipitously increase the temperatures. For utilizing the reduced false air, a further reduction in inlet temperature would be required and thus allow for reocvery of more waste heat. By partially sealing the inlet a solution must be found to allow for cool transport air during STD production.

So, how will the false air intrusion change with the WHRU installation? The modelled system uses the same O_2 concentrations, hence the same flow rates. But several mechanisms could affect the flow rate, where the AFM inlet pressure is a key parameter. How this will change with the installation of the WHRU depends on the pressure needed to transport the required gas from the bypass duct to the inlet, thus preventing the gas being routed directly to the filters. ESP inlet pressure will be vital to set the overall system pressure which will allow for sufficient flow rate to the AFM without a too low inlet pressure. A CFD analysis would benefit this question.

6.2.2 Reduced saturation temperature

With the WHRU in operation, the GCT is shut down to increase the hot gas temperature. This will reduce the H_2O load in the gas at the AFM inlet and thereby reduce the saturation temperature. This in turn could benefit the heat recovery process by lowering the AFM inlet temperature. The critical area regarding low temperatures is downstream of the AFM where temperatures today often drop to ≈52-55°C during LA production and from ≈60-70°C during STD production. A further reduction during LA production can cause condensation and problems with mud formation. With the reduced water load, this temperature could be lowered

as described in chapter 5.4 and therefore, allow for additional heat recovery. An inlet temperature of 183.5 is calculated to produce an outlet temperature at the new saturation point, at 44°C. This reduction would require a prolonged residence time for the raw materials to achieve complete evaporation of the water, but if this increase supersedes the present residence time should be investigated further. A prolonged residence time, relative to present, would impact the production capacity negatively and would therefore be undesirable.

For STD production, the lowered saturation temperature cannot be utilized since all the hot gas is already utilized for heat recovery. By increasing the heat recovery capacity in the WHRU available heat could be utilized during both STD and LA production. This holds for both temperature reduction due to a lowered saturation point and for a reduction in false air.

6.2.3 Operational constraints limiting the production

To achieve a successful integration of the WHRU system the impact on the existing facility must be as little as possible, with the production capacity being the key parameter. The temperature range in use today will be achievable by mixing the hot preheater gas with the cooled gas from the WHRU, and the flow rate will be sufficient to cover all normal conditions. The challenge will be in balancing the system with the correct pressures to reach the required flow rates and temperatures.

7 Conclusion

Extending the current system with a WHRU will affect the operation of the raw meal production by changing temperatures, flow rates and how the gas flow is controlled. For STD production the AFM inlet temperature is reduced to 170°C which is the WHRU outlet temperature. This will reduce the outlet temperature but under normal conditions condensation should not be an issue. The reduced H_2O load reduces the saturation temperature as seen in Table 5.7 and further reduces the likelihood for condensation. So increasing the STD inlet temperature should not be necessary. During production of LA the temperature is controlled freely by adjusting the WHRU fan speed to match the present temperatures and the production capacity should remain unchanged.

By sealing of the AFM inlet the false air can be reduced or even removed. A complete removal will be undesirable since this will cause a gas deficit in addition to the outlet temperatures rising to unwanted levels. A partial sealing will be a better solution where 2.66MW could be recovered during LA production. Anyhow, during STD production this will only lead to increased outlet temperatures and no additional heat recovery. Partial sealing would be beneficial if it could be utilized during both production types.

Based on these calculations, with the planned WHRU installation, sealing of the AFM inlet will only enhance the recovery for LA production.

Further the reduced water load in the hot gas from the preheater will reduce the saturation temperature, thus allow for a reduction in the AFM in- and outlet temperature. If the raw materials residence time is sufficient, the inlet temperature can be reduced during LA production, and depending on the needed residence time, an additional 1.92MW can recovered.

The outline of these results is that the raw meal production capacity should not change with the installation of the WHRU. With the reduced H_2O content in the hot gas the saturation point will drop and allow for a lower outlet temperature. Further work and tests should be performed to conclude on residence time for complete evaporation at lower temperatures.

References

[1] Johanna Lehne and Felix Preston, "Making Concrete Change: Innovation in Low-carbon Cement and Concrete," 2018.

[2] Norcem. "Materialregnskap og utslipp." https://www.norcem.no/no/materialregnskap_brevik (accessed 20.1, 2022).

[3] J. Silva. *Heat and mass balance at Norcem Brevik 2018*.

[4] EngineeringToolbox. "Convective Heat Transfer." https://www.engineeringtoolbox.com/convective-heat-transfer-d_430.html (accessed 3.4, 2022).

[5] J. M. Smith, H.C. Van Ness, M. M. Abbott, and M. T. Swihart, *Introduction to Chemical Engineering Thermodynamics*, 8th ed. McGraw-Hill Education, 2018.

[6] Testo. "Testo 340 Instruction manual." https://static-int.testo.com/media/17/0f/6aa36530c364/testo-340-Instruction-Manual.pdf (accessed 1.4, 2022).

[7] *Stationary source emissions: Determination of the water vapour in ducts*, Swedish Standard Institute, 2017.

[8] Testo. "Air flow measurements in ducts according to DIN EN 12599." https://static-int.testo.com/media/5e/bf/7203dd113db1/jp_practical_guide_testo-400-AirFlow.pdf (accessed 1.3, 2022).

[9] J. R. Elliott and C. T. Lira, *Introductory Chemical Engineering Thermodynamics*. Pearson, 2012.

Appendices

Appendix A	Thesis Project Description
Appendix B	3D Model
Appendix C	Heat capacity constants used in the calculations
Appendix D	Heat loss calculations
Appendix E	Antoine equation constants
Appendix F	Differential pressure for velocity measurements
Appendix G	Duct diameters
Appendix H	Manual O_2 measurements and conversion between dry and wet basis
Appendix I	Procedure for fitting of ΔT values in the AFM system
Appendix J	Calculation steps STD
Appendix K	Process data plots
Appendix L	Calculation of ESP3 O_2 online measurement deviance
Appendix M	Flowsheet STD production
Appendix N	Flowsheet LA production
Appendix O	Flowsheet STD production WHRU
Appendix P	Flowsheet LA production WHRU
Appendix Q	Flowsheet STD production WHRU reduced false air
Appendix R	Flowsheet LA production WHRU reduced false air
Appendix S	Flowsheet LA production WHRU and reduced saturation temperature

Appendix A Thesis Project description

FMH606 Master's Thesis

Title: The impact of waste heat recovery unit installation on the operation and control of the raw meal department at Norcem Brevik

USN supervisor: Lars-André Tokheim

External partner: Norcem Brevik

Task background:
A post-combustion CO_2 capture plant is to be installed at Norcem's cement plant in Brevik and will be in operation from 2024. A key feature of the Norcem CCS project is the utilization of waste heat from the cement production process for regeneration of the chemical solvent in the capture plant. The waste heat utilization requires installation of several waste heat recovery units (WHRU). One of these (WHRU 2) will be located in the raw meal department (RM), see Figure 1.

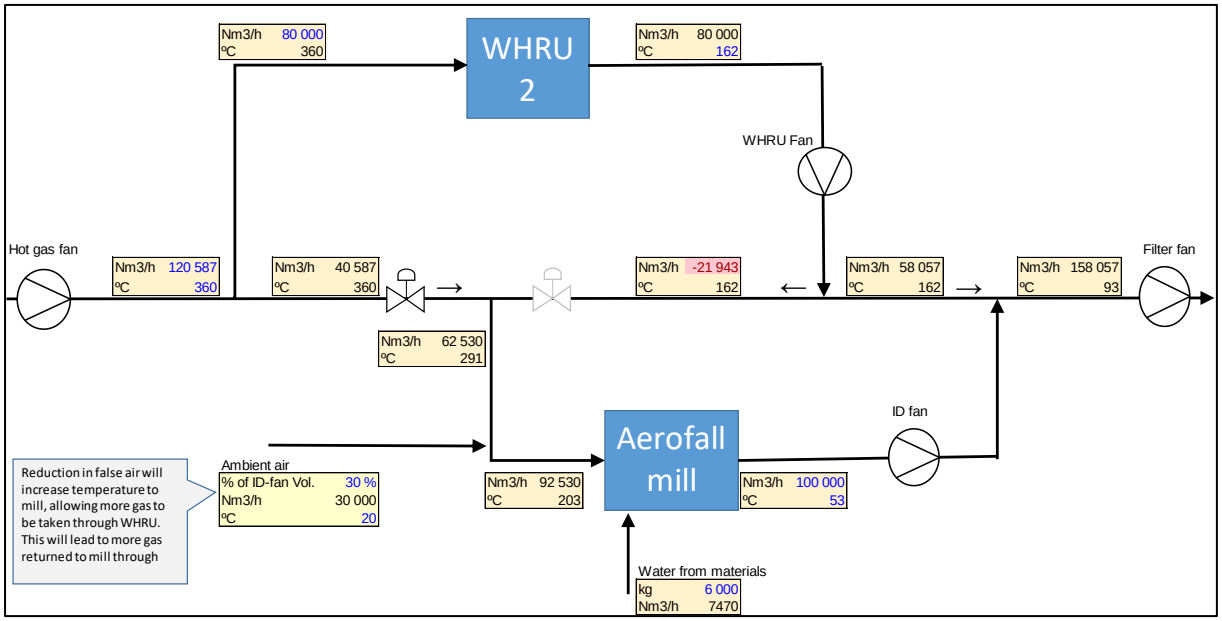

Figure 1: Flow sheet with approximate gas flow rates and temperatures in the raw meal department (example for low-alkali production).

Today the temperature of the exhaust gas from the preheater towers is reduced to typically 290 °C (for LA production) by injection of water in conditioning tower 2 (CT2; not shown in Figure 1). However, after installation of the capture plant, CT2 will not be used, and the gas

will be sent to the raw meal department without pre-cooling, which means an expected RM inlet temperature of about 360 °C. The purpose of this is to maximize the amount of heat transfer in WHRU 2.

Today, there is a significant inflow of false air at the AFM inlet, and this air stream increases the total gas flow rate and reduces the inlet gas temperature to the AFM. The amount of false air is partly a function of the pressure at the AFM inlet. However, this pressure may change in the future as a new valve is planned to be installed upstream of the AFM (see Figure 1) in order to improve the control of the gas flow going into the AFM. To obtain a better gas flow control it may be an option to increase the pressure upstream of the new valve or to reduce the pressure at the AFM inlet. The latter will impact the false air intrusion, and it may be necessary to modify the AFM inlet to reduce the amount of false air.

The picture is complicated by the fact that the RM operational values are quite different depending on whether standard raw meal (STD) or low-alkali raw meal (LA) is produced. This is due to different grindability of the raw materials used during STD and LA production.

The key question to answer is the following: Will the drying capacity or the raw meal production capacity change with the new system in operation?

To answer the key question, additional questions should be addressed:

- What is the gas flow rates, temperatures and pressures in the RM system today (for STD and LA production), and how will they change after the new system is in operation?
- How much false air is there in the system today, and how will it change with a new way to operate RM?
- Should the false air at AFM inlet be reduced by constructional changes? How will that affect the operation of the system?
- Which operational constraints will limit the operation?

Task description:

Possible sub-tasks may be:

- Describe the current and future RM process, for both STD and LA production, including typical process values and operational constraints
- Describe how the raw meal production rate and quality is controlled today, and will be controlled in the future

- Make process flow diagrams with typical flow rates, temperatures and pressures for the current and future system
- If necessary/useful, measure gas flow rates and oxygen concentrations in different parts of the system to determine unknown values
- Make a mathematical model for false air intrusion at the AFM inlet
- Make a mass and energy balance of the RM department, both for current operation and future operation (with WHRU 2 installed)
- Investigate how the new system may impact the drying capacity and the raw meal production capacity
- Investigate the impact of variable false air flow rates on the operation of the current and future system
- Describe the operational impact of changeover between STD and LA production and startup/shutdown of the CO_2 capture system

Student category: Reserved for Fredrik Høibjerg (PT student and Norcem employee)

The task is suitable for online students (not present at the campus): No

Practical arrangements:

Documentation is available from the Norcem CCS project (e.g. Tor Gautestad and Otto Bade). Part of the work (e.g. measurements) will be carried out at the plant in Brevik.

Supervision:

As a general rule, the student is entitled to 15-20 hours of supervision. This includes necessary time for the supervisor to prepare for supervision meetings (reading material to be discussed, etc).

Signatures:

Supervisor (date and signature): 28 January 2022, Lars Andre Tokheim

Student (write clearly in all capitalized letters): FREDRIK HØIBJERG KASIN

Student (date and signature): 28 January 2022, Fredrik H Kasin

Appendix B 3D Model

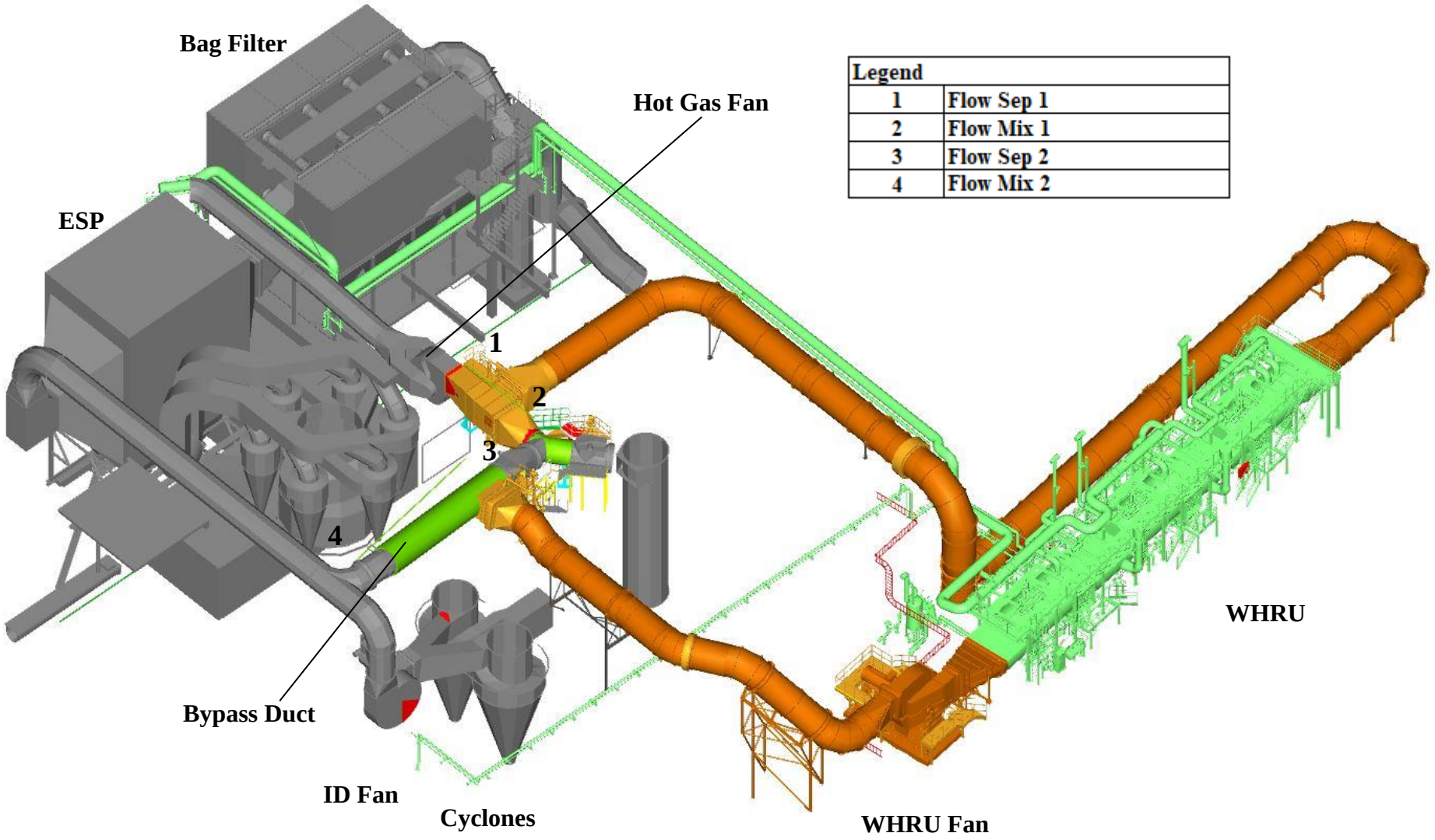

Legend	
1	Flow Sep 1
2	Flow Mix 1
3	Flow Sep 2
4	Flow Mix 2

Appendix C Heat capacity constants used in the calculations

Heat Capacity Polynomial Constants[5]

Component	**A**	**10^3 B**	**10^6 C**	**10^{-5} D**
CO_2	5.457	1.045	-	-1.157
O_2	3.639	0.506	-	-0.227
N_2	3.280	0.593	-	0.040
H_2O	3.470	1.450	-	0.121
Limestone	12.072	2.637	-	-3.120

Appendix D Heat loss calculations

Measured temperatures and heat transfer coefficient for the different equipment.

Location	**Area**	v	T_S	T_A	h_c $[W/m^2°C]$
AFM	250	2	33	20	26.2
Coarse Sep	110	0	40	20	12.12
Cyclones	301	0	50	20	12.12

Calculated loss

Location	**Units**	**Loss**
AFM	[kW]	85.2
Coarse Sep	[kW]	26.7
Cyclones	[kW]	109.4

Appendix E Antoine equation constants

Antoine equation constants for water with pressure in mmHg and temperature in °C [9].

Component	**A**	**B**	**C**
Water	8.07131	1730.63	233.426

Appendix F Differential pressure for velocity measurements

STD production

1				
Location	**Units**	**Stream 1**	**Stream 12**	**Stream 13**
1	[mbar]	2.58	0.57	5.11
2	[mbar]	3.18	0.62	5.04
3	[mbar]	4.36	0.65	6.36
4	[mbar]	4.09	0.79	5.99
5	[mbar]	3.22	0.40	5.71
Average	[mbar]	3.486	0.606	5.642
2				
Location	**Units**	**Stream 1**	**Stream 12**	**Stream 13**
1	[mbar]	2.90	0.56	5.28
2	[mbar]	3.13	0.68	4.94
3	[mbar]	3.57	0.67	6.43
4	[mbar]	3.714	0.61	5.4
5	[mbar]	3.56	0.44	4.9
Average	[mbar]	3.374	0.592	5.39

LA production

1				
Location	**Units**	**Stream 1**	**Stream 12**	**Stream 13**
1	[mbar]	3.45	0.82	4.10
2	[mbar]	3.44	0.75	4.05

3	[mbar]	3.72	0.68	4.83
4	[mbar]	3.33	0.44	4.5
5	[mbar]	3.20	0.35	4.43
Average	[mbar]	3.428	0.608	4.43
2				
Location	**Units**	**Stream 1**	**Stream 12**	**Stream 13**
1	[mbar]	2.96	0.90	3.72
2	[mbar]	3.03	0.78	4.04
3	[mbar]	4.11	0.52	4.99
4	[mbar]	3.1	0.53	4.24
5	[mbar]	3.52	0.40	4.33
Average	[mbar]	3.344	0.626	4.264

Final averaged values

	Units	**Stream 1**	**Stream 12**	**Stream 13**
STD	[mbar]	3.430	0.599	5.516
LA	[mbar]	3.386	0.617	4.323

Appendix G Duct diameters

Duct diameters

	Units	Stream 1	Stream 12	Stream 13
Diameter	[mm]	1 750	2 000	2 000

Department inlet

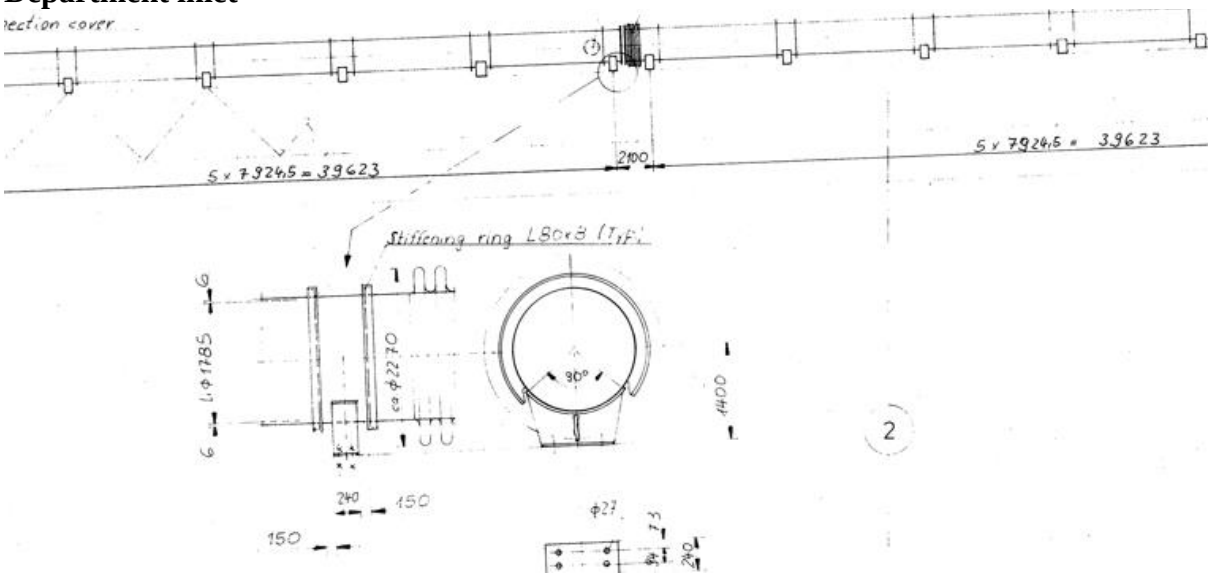

Bypass- and ESP ducting

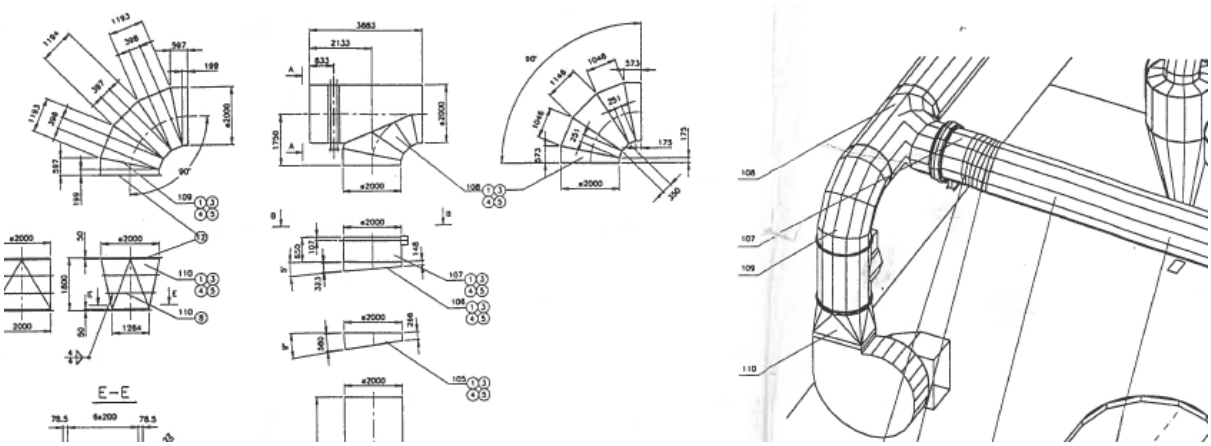

Appendix H Manual O_2 measurements and conversion between dry and wet basis

The H_2O fraction in stream 13 is calculated by using the H_2O balance over the mixing point downstream of the AFM and bypass duct. Fractions in stream 11 and 12 are known from the H_2O measurements and the fraction in stream 13 is solved for.

$$\dot{V}_{g,13} * y_{H_2O,13} = \dot{V}_{g,11} * y_{H_2O,11} + \dot{V}_{g,12} * y_{H_2O,12}$$

The H_2O fraction in stream 14 is calculated by solving a system of equations due to 4 unknowns ($\dot{V}_{g,14}$, $\dot{V}_{FA}$, y_{H_2O}, y_{O_2}). The flow rate in stream 14 is found by combining the equations described in chapter 4.3 and given below. With the flow rate established the H_2O-, and O_2 fractions can be calculated by solving the BF component balances. For simplicity, both equations are given below.

$$y_{O_{2,dry}}\left(1 - \frac{y_{H_2O,15} * \dot{V}_{g,15}}{\dot{V}_{g,14}}\right) * \dot{V}_{g,14} + y_{O_2,FA}\left(\dot{V}_{g,15} - \dot{V}_{g,14}\right) = y_{O_2,15} * \dot{V}_{g,15}$$

$$y_{H_2O,1} * \dot{V}_{g,14} = y_{H_2O,15} * \dot{V}_{g,15}$$

$$y_{O_2,14} * \dot{V}_{g,14} = y_{O_2,15} * \dot{V}_{g,15}$$

STD	**Units**	**$O_{2,\ Dry}$**	**H_2O**	**$O_{2,\ Wet}$**
$y_{O_2,1}$	[%]	0.0658	0.2159	0.0516
$y_{O_2,11}$	[%]	0.1488	0.0973	0.1343
$y_{O_2,13}$	[%]	0.1272	0.1330	0.1109
$y_{O_2,14}$	[%]	0.1285	0.1287	0.1124
$y_{O_2,15}$	[%]	0.1309	0.1267	0.1143

LA	**Units**	**$O_{2,\ Dry}$**	**H_2O**	**$O_{2,\ Wet}$**
$y_{O_2,1}$	[%]	0.0783	0.1762	0.0645
$y_{O_2,11}$	[%]	0.1549	0.1159	0.1369

$y_{O_2,13}$	[%]	0.1278	0.1358	0.1104
$y_{O_2,14}$	[%]	0.1289	0.1306	0.1121
$y_{O_2,15}$	[%]	0.1318	0.1251	0.1152

Appendix I Procedure for fitting of ΔT values in the AFM system

Rearranging the ΔT equations for implementation in the AFM-, coarse separator and cyclones energy balance.

$$T_{RM8} = T_8 - \Delta T_8$$
$$T_{RM9} = T_9 - \Delta T_9$$
$$T_{RM19} = T_8 - \Delta T_{19}$$
$$T_{RM20} = T_{10} - \Delta T_{20}$$

The AFM energy balance equation will be as follows

$$\dot{m}_{g,7} * Cp_{g,7} * (T_7 - T_8) + P_{mill} = \left(\dot{m}_{RM,18} * \left(1 - w_{H_2O,18}\right)\right) * Cp_{RM} * \left(T_8 - \Delta T_8 - T_{RM,18}\right) + \dot{m}_{RM,18} * w_{H_2O,15} * \left(Cp_{H_2O,vap} * \left(T_8 - T_{RM,18}\right) + \Delta H_{vap}\right) + \dot{m}_{FA,17} * Cp_{FA} * (T_8 - T_{FA}) + Q_{Loss,AFM}$$

Coarse separator is changed to the following

$$\dot{m}_{g,8} * Cp_{g,8} * (T_8 - T_9) = \dot{m}_{RM,19} * Cp_{RM,19} * \left(-\Delta T_{19} + T_{RM,8}\right) + \dot{m}_{RM,9} * Cp_{RM,9} * (T_9 - \Delta T_9 - T_8 + \Delta T_8) + Q_{Loss,Sep}$$

Cyclone's energy balance with the ΔT's implemented

$$\dot{m}_{g,9} * Cp_{g,9} * (T_9 - T_{10}) = \dot{m}_{RM,20} * Cp_{RM,20} * (T_{10} - \Delta T_{20} - T_9 + \Delta T_9) + \dot{m}_{RM,10} * Cp_{RM,10} * (T_{10} - T_9 + \Delta T_9) + Q_{Loss,Cyc}$$

Then by performing the iterative procedure described in chapter 4.5.1 the following ΔT's are established for STD and LA production.

Appendix J Calculation steps STD

Solving of the system based on reference values from STD production allows for validation of the model and ensures the consistency of the output. For the reference case the input values are given in Table 5.2. By using these parameters the mass flow rate in stream 1 is calculated by rearranging and combining the total mass flow (3.1) and the total oxygen balance (3.28). Conversion between mass and volumetric flow is done with ideal gas law. The raw material H_2O fraction is calculated based on the AFM in- and outlet stream H_2O concentration.

$$V_{m,ref} = (V_2 - V_1) * \frac{T_N}{T_m}$$

$$V_{m,ref,1} = 0.107 * \frac{273.15}{273.15 + 20.775} \qquad V_{m,ref,11} = 0.168 * \frac{273.15}{273.15 + 32.7}$$

$$V_{m,ref,1} = 0.0994 \qquad V_{m,ref,11} = 0.150$$

Calculating H_2O concentration in the flue gas

$$y_{H_2O} = \frac{\frac{m_{H_2O} * V_{mol}}{MM}}{\frac{m_{H_2O} * V_{mol}}{MM} + V_{m,ref}}$$

$$y_{H_2O,1} = \frac{\frac{22 * 22.4 * 10^{-3}}{18}}{\frac{22 * 22.4 * 10^{-3}}{18} + 0.0994} \qquad y_{H_2O,11} = \frac{\frac{13 * 22.4 * 10^{-3}}{18}}{\frac{13 * 22.4 * 10^{-3}}{18} + 0.150}$$

$$y_{H_2O,1} = 0.2159 \qquad y_{H_2O,11} = 0.0973$$

Calculating the resulting vapor from evaporation of water in raw materials and deciding the water weight fraction in the materials. Values for gas flow used are based on measurements during the sampling.

$$\dot{V}_{H_2O,vap} = y_{H_2O,11} * \dot{V}_{g,11} - y_{H_2O,1} * \dot{V}_{g,7}$$

$$\dot{V}_{H_2O,vap} = 0.0973 * 195\,459 - 0.2159 * 79\,083 = 1\,944\ Nm^3/h$$

$$\dot{V}_{H_2O,vap} = \frac{R * T_N * (w_{H_2O} * \dot{m}_{RM,18})}{MM * p_N}$$

$$1\,944 = \frac{8.314 * 273.15 * (w_{H_2O} * 200\,000)}{0.018 * 101\,325}$$

$$w_{H_2O} = 0.007$$

This value is then set for the material feed and used when solving the model. The updated vapor from evaporation is

$$\dot{V}_{H_2O,vap} = \frac{8.314 * 273.15 * (0.007 * 160\,000)}{0.018015 * 101\,325} = 1\,393\,\frac{Nm^3}{h}$$

Deciding the hot gas flow rate into the raw meal department using total O_2 and mass balance.

$$\dot{V}_{g,1} = \frac{\left(\dot{V}_{g,16} - \dot{V}_{H_2O,vap}\right) * y_{O_2,FA} - y_{O_2,16} * \dot{V}_{g,16}}{y_{O_2,FA} - y_{O_2,1}}$$

$$\dot{V}_{g,1} = \frac{(282\,534 - 1\,393) * 0.21 - 0.1143 * 282\,534}{0.21 - 0.0451} = 162\,195\,\frac{Nm^3}{h}$$

Then the total CO_2 balance is used to calculate the volume fraction at the inlet and thereby determining the gas composition.

$$y_{CO_2,1} = \frac{y_{CO_2,16} * \dot{V}_{g,16}}{\dot{V}_{g,1}}$$

$$y_{CO_2,1} = \frac{0.1077 * 282\,534}{162\,195} = 0.1876$$

$$y_{H_2O,1} = \frac{y_{H_2O,16} * \dot{V}_{g,16} - \dot{V}_{H_2O,vap}}{\dot{V}_{g,1}}$$

$$y_{H_2O,1} = \frac{0.1267 * 282\,534 - 1\,393}{162\,195} = 0.212$$

Stream 1 molar mass

$$MM_{g,1} = \sum y_i * MM_i$$

$$MM_{g,1} = \frac{0.0451 * 31.99 + 0.2159 * 18.015 + 0.1877 * 44.01 + 0.5513 * 28.014}{1000}$$

$$MM_{g,1} = 0.02903$$

Using the calculated molar mass to calculate the mass flow in stream 1.

$$\dot{m}_{g,1} = \frac{\dot{V}_{g,1} * MM_{g,1} * p_N}{R * T_N}$$

$$\dot{m}_{g,1} = \frac{162\,195 * 0.02903 * 101\,325}{8.314 * 273.15} = 210\,082 kg/h$$

By establishing the flow rate coming into the raw meal department the total false air flow rate can be calculated by rearranging the system total O_2 balance. The conversion between volume and mass flow is as above with corresponding molar mass.

$$\dot{V}_{FA} = \frac{y_{O_2,16} * \dot{V}_{g,16} - y_{O_2,1} * \dot{V}_{g,1}}{y_{O_2,FA}}$$

$$\dot{V}_{FA} = \frac{0.1143 * 282\,534 - 0.0451 * 162\,195}{0.21}$$

$$\dot{V}_{FA} = 118\,946\ \frac{Nm^3}{h} \qquad \dot{m}_{FA} = 154\,064 \frac{kg}{h}$$

Further to establish the sources of false air and their flowrate the measurements shown in Table 4.4 are used to calculate the false air intrusion at the ESP and bag filter. This is achieved by using the component balances in equation (3.37) and (3.38) in combination with the mass balances in equation (3.6) and (3.7). The same procedure shown below is repeated for the ESP.

$$\dot{V}_{g,14} = \frac{y_{O_2,FA} * \dot{V}_{g,15} - y_{O_2,15} * \dot{V}_{g,15}}{y_{O_2,FA} - y_{O_2,14}}$$

$$\dot{V}_{g,14} = \frac{0.21 * 282\,534 - 0.1143 * 282\,534}{0.21 - 0.1124}$$

$$\dot{V}_{g,14} = 277\,033 \frac{Nm^3}{h} \qquad \dot{m}_{g,14} = 358\,827 \frac{kg}{h}$$

$$\dot{V}_{g,13} = 272\,840 \frac{Nm^3}{h} \qquad \dot{m}_{g,13} = 353\,395 \frac{kg}{h}$$

$$\dot{V}_{FA,24} = \dot{V}_{g,15} - \dot{V}_{g,14}$$

$$\dot{V}_{FA,24} = 5\,500 \frac{Nm^3}{h} \qquad \dot{m}_{FA,24} = 7\,124 \frac{kg}{h}$$

$$\dot{V}_{FA,23} = 4\,193 \frac{Nm^3}{h} \qquad \dot{m}_{FA,23} = 5\,431 \frac{kg}{h}$$

With the total false air intrusion known as well as in the filters, the mill inlet false air is known due to assumption of false air at AFM inlet and in filters. This is calculated by solving equation (3.2).

$$V_{FA,17} = \dot{V}_{FA} - \dot{V}_{FA,24} - \dot{V}_{FA,23}$$

$$\dot{V}_{FA,17} = 109\,252 \frac{Nm^3}{h} \qquad \dot{m}_{FA,17} = 141\,509 \frac{kg}{h}$$

Changes in O_2 and CO_2 concentration due to false air in ESP and bag filter is calculated as shown below.

$$y_{CO_2,14} = \frac{y_{CO_2,15} * \dot{V}_{g,15}}{\dot{V}_{g,14}}$$

$$y_{CO_2,14} = \frac{0.1077 * 282\,534}{277\,033}$$

$$y_{O_2,14} = \frac{y_{O_2,15} * \dot{V}_{g,15} - y_{O_2,FA} * \dot{V}_{FA,BF,24}}{\dot{V}_{g,14}}$$

$$y_{O_2,14} = \frac{0.1143 * 282\,534 - 0.21 * 5\,500}{277\,033}$$

$$y_{CO_2,14} = 0.1098 \qquad y_{CO_2,13} = 0.1115$$

$$y_{O_2,14} = 0.1124 \qquad y_{O_2,13} = 0.1109$$

To approximate the gas heat capacity in the AFM values based on measurements are used in the calculations of gas composition. This way a heat capacity is calculated prior to solving of the model, but this will be a static value in the model.

$$y_{O_2,8} = \frac{y_{O_2,FA} * \dot{V}_{FA,17} + y_{O_2,7} * \dot{V}_{g,7}}{\dot{V}_{g,8}}$$

$$y_{O_2,8} = \frac{0.21 * 116\,375 + 0.051 * 79\,083}{195\,459} = 0.145$$

$$y_{CO_2,8} = \frac{y_{CO_2,7} * \dot{V}_{g,7}}{\dot{V}_{g,8}}$$

$$y_{CO_2,8} = \frac{0.1810 * 79\,083}{195\,459} = 0.073$$

$$\langle Cp \rangle = \frac{\left(A + \frac{B}{2} * (T + T_0) + \frac{C}{3}(T^2 + T_0^2 + T * T_0) + \frac{D}{T * T_0}\right) * R}{MM}$$

$$Cp_{O_2} = \frac{\left(3.639 + \frac{0.506 * 10^{-3}}{2}(473.15 + 341.15) + \frac{-0.227 * 10^5}{473.15 * 341.15}\right) * 8.314}{31.999} = 0.962$$

$$Cp_{CO_2} = \frac{\left(5.457 + \frac{1.045 * 10^{-3}}{2}(473.15 + 341.15) + \frac{-.1.157 * 10^5}{473.15 * 341.15}\right) * 8.314}{44.009}$$

$$= 0.976$$

$$Cp_{H_2O} = \frac{\left(3.470 + \frac{1.45 * 10^{-3}}{2}(473.15 + 341.15) + \frac{0.121 * 10^5}{473.15 * 341.15}\right) * 8.314}{18.015} = 1.93$$

$$Cp_{N_2} = \frac{\left(3.28 + \frac{0.593 * 10^{-3}}{2}(473.15 + 341.15) + \frac{0.04 * 10^5}{471.15 * 341.15}\right) * 8.314}{28.014} = 1.052$$

With the final mixture heat capacity being calculated as shown below

$$Cp_{Mix}^{ig} = \sum y_i * Cp_i$$

$$Cp_{Mix}^{ig} = 0.145 * 0.962 + 0.073 * 0.976 + 0.0973 * 1.93 + 0.685 * 1.052 = 1.119 \frac{kJ}{kgK}$$

For the second mixing point, the bypass stream 12 and the mill outlet stream 11 flow rate is unknown and must be determined. This is achieved with the AFM system energy balances given in equations (3.20) to (3.22). Here the raw material streams must be identified and calculated prior to solving the energy balances. Using the mill total feed rate and the coarse separator efficiency the flow rate in stream 9 and 19 is calculated.

$$\dot{m}_{RM,19} = \dot{m}_{RM,18} * \left(1 - w_{H_2O}\right) * \eta_{Sep}$$

$$\dot{m}_{RM,19} = 160\,000 * (1 - 0.007) * 065 = 103\,272 \frac{kg}{h}$$

$$\dot{m}_{RM,9} = \dot{m}_{RM,18} - \dot{m}_{RM,19}$$

$$\dot{m}_{RM,9} = 160\,000 - 103\,272 = 56\,728 \frac{kg}{h}$$

From Table 3.1 the cyclones efficiency is set to 90% which corresponds to the following mass flow rates.

$$\dot{m}_{RM,20} = \dot{m}_{RM,9} * \eta_{Cyc}$$

$$\dot{m}_{RM,20} = 56\,728 * 0.90 = 51\,055 \frac{kg}{h}$$

$$\dot{m}_{RM,10} = \dot{m}_{RM,9} - \dot{m}_{RM,20}$$

$$\dot{m}_{RM,10} = 56\,7283 - 51\,055 = 5\,672\,\frac{kg}{h}$$

Temperatures up- and downstream the AFM system are known from online measurements and by rearranging the coarse separator- and cyclone energy balances, (3.21) and (3.22), as functions of temperature in stream 9 and 8 the AFM energy balance (3.20) can be solved for the mass flow rate in stream 7.

$$T_9 = \Big(\Big(\big(\Delta T_9 + T_{RM,20}\big) * \dot{m}_{RM,20} + \dot{m}_{RM,10} * (T_{10} + \Delta T_9)\Big) * Cp_{RM} + \dot{m}_{g,8} * Cp_{g,AFM} * T_{10} + \dot{Q}_{Cyc}\Big) \;/\; \Big(\big(\dot{m}_{RM,10} + \dot{m}_{RM,20}\big) * Cp_{RM} + \dot{m}_{g,8} * Cp_{g,AFM}\Big)$$

$$T_8 = \Big(\Big((T_9 + \Delta T_8 - \Delta T_9) * \dot{m}_{RM,9} + \dot{m}_{RM,19} * \big(\Delta T_8 + T_{RM,19}\big)\Big) * Cp_{RM} + \dot{m}_{g,8} * Cp_{g,AFM} * T_9 + \dot{Q}_{Sep}\Big) \;/\; \Big(\big(\dot{m}_{RM,9} + \dot{m}_{RM,19}\big) * Cp_{RM} + \dot{m}_{g,8} * Cp_{g,AFM}\Big)$$

Then setting up the expression for gas mass flow in stream 8 and substituting this in the above equations.

$$\dot{m}_{g,8} = \dot{m}_{g,7} + \dot{m}_{FA,AFM,17} + (w_{H_2O} * \dot{m}_{RM,18})$$

In equation (3.48) (3.51) the relationship between the gas- and raw material temperature is defined, where the ΔT is based on local measurements. See Appendix I for values.

Then by rearranging the ΔT equations as functions of the raw material temperature this unknown value can be replaced in the AFM system energy balances. T9 and the expression for mass flow in stream 8 is substituted into T8, which gives

$$
\begin{aligned}
T_8 = \Big(& T_{10}\left(\dot{m}_{g,7} + \dot{m}_{FA,AFM,17} + w_{H_2O} * \dot{m}_{RM,18}\right)^2 Cp_{g,AFM}{}^2 \\
& + \left(\dot{m}_{g,7} + \dot{m}_{FA,AFM,17} + w_{H_2O} * \dot{m}_{RM,18}\right) \\
& * \Big(\Big((T_{10} + \Delta T_8 - \Delta T_9)\dot{m}_{RM,9} + T_{10} * \dot{m}_{RM,10} + (T_{RM,20} + \Delta T_9)\dot{m}_{RM,20} \\
& + \Delta T_9 * \dot{m}_{RM,10} + \dot{m}_{RM,19}(T_{RM,19} + \Delta T_8) \Big) Cp_{RM} + \dot{Q}_{Cyc} + \dot{Q}_{Sep} \Big) Cp_{g,AFM} \\
& + \Big(\Big((T_{10} * \dot{m}_{RM,10} + (T_{RM20} + \Delta T_8)\dot{m}_{RM.20} + \Delta T_8 * \dot{m}_{RM,10})\dot{m}_{RM,9} \\
& + \dot{m}_{RM,19}(\dot{m}_{RM,20} + \dot{m}_{RM,10})(T_{RM,19} + \Delta T_8) \Big) Cp_{RM} + \dot{Q}_{Cyc} * \dot{m}_{RM,9} \\
& + \dot{Q}_{Sep}(\dot{m}_{RM,20} + \dot{m}_{RM,10}) \Big) Cp_{RM} \Big) \\
& / \Big(\Big(Cp_{g,AFM}\left(\dot{m}_{g,7} + \dot{m}_{FA,AFM,17} + w_{H_2O} * \dot{m}_{RM,18}\right) \\
& + Cp_{RM}(\dot{m}_{RM,19} + \dot{m}_{RM,9}) \Big) \Big(Cp_{g,AFM}\left(\dot{m}_{g,7} + \dot{m}_{FA,AFM,17} + w_{H_2O} * \dot{m}_{RM,18}\right) \\
& + Cp_{RM}(\dot{m}_{RM,20} + \dot{m}_{RM,10}) \Big) \Big)
\end{aligned}
$$

The expression for T8 is substituted into the AFM energy balance where the system is solved for the gas mass flow in stream 7. This is calculated using the solve function in Maple with an assumption parameter to return only the positive value.

$$
\begin{aligned}
\dot{m}_{g,7} * Cp_{g,7} * (T_7 - T_8) + P_{mill} & \\
= \left(\dot{m}_{RM,18} * \left(1 - w_{H_2O,18}\right)\right) * Cp_{RM} * \left(T_8 - \Delta T_8 - T_{RM,18}\right) + \dot{m}_{RM,18} & \\
* w_{H_2O,15} * \left(Cp_{H_2O,vap} * \left(T_8 - T_{RM,18}\right) + \Delta H_{vap}\right) + \dot{m}_{FA,17} * Cp_{FA} & \\
* (T_8 - T_{FA}) + Q_{Loss,AFM} &
\end{aligned}
$$

This yields the following results for the AFM required inlet flowrate.

$$\dot{V}_{g,7} = 80\,429\ \frac{Nm^3}{h} \qquad\qquad \dot{m}_{g,7} = 104\,176\ \frac{kg}{h}$$

This in turn allows for calculation of stream 8 by using equation (3.4), and by that fully defining the AFM system flow rates.

$$\dot{m}_{g,8} = \dot{m}_{g,7} + \dot{m}_{FA,AFM,17} + (w_{H_2O} * \dot{m}_{RM,18})$$

$$\dot{m}_{g,8} = 104\,176 + 141\,509 + (0.007 * 160\,000) = 246\,805\,\frac{kg}{h}$$

$$\dot{V}_{g,8} = 191\,075\,\frac{Nm^3}{h}$$

The temperatures in stream 8 and 9 is calculated using equations (3.21) and (3.22).

$$T_9 = \Big(\Big(\big(\Delta T_9 + T_{RM,20}\big) * \dot{m}_{RM,20} + \dot{m}_{RM,10} * (T_{10} + \Delta T_9)\Big) * Cp_{RM} + \dot{m}_{g,8} * Cp_{g,AFM} * T_{10} + \dot{Q}_{Cyc}\Big) \;/\; \Big(\big(\dot{m}_{RM,10} + \dot{m}_{RM,20}\big) * Cp_{RM} + \dot{m}_{g,8} * Cp_{g,AFM}\Big)$$

$$T_9 = \frac{\big((11 + 57.7)51\,055 + 5\,672 * (67 + 11)\big)0.74 + 246\,805 * 1.119 * 67 + 100}{(5\,672 + 51\,055)0.74 + 246\,805 * 1.119}$$

$$T_9 = \; 68°C$$

Corresponding values are used in the equation for T8 which gives the following temperature

$$T_8 = 71.84$$

Since the flow rate into the department and AFM is known the bypass-duct flow rate is calculated with equation (3.3).

$$\dot{V}_{g,12} = \dot{V}_{g,1} - \dot{V}_{g,7}$$

$$\dot{V}_{g,12} = 162195 - 80\,429 = 81\,766$$

$$\dot{m}_{g,12} = 105\,906\;\frac{kg}{h}$$

The temperature in stream 11, downstream of the ID fan, is unknown and is calculated using equation (3.56) and (3.57). R/Cp value is estimated, assuming air, to be 0.2857 and the fan efficiency to 75%[5].

$$T'_{11} = T_{10} * \left(\frac{P_{11}}{P_{10}}\right)^{R/C_p}$$

$$T'_{11} = 68 * \left(\frac{101325}{90000}\right)^{0.2857} = 70.4$$

$$T_{11} = 68 + \frac{70.4 - 68}{0.70} = 74.1$$

Temperature downstream of the second mixing point in stream 13 is then calculated using equation (3.23). In stream 14 and 15 the temperature is calculated using equation (3.24) and (3.25), respectively.

$$T_{13} = \frac{T_{11} * \dot{m}_{g,11} * Cp_{g,AFM} + T_{12} * \dot{m}_{g,12} * Cp_{g,In}}{\dot{m}_{g,11} * Cp_{g,AFM} + \dot{m}_{g,12} * Cp_{g,In}}$$

$$T_{13} = \frac{74.1 * 246\,805 * 1.119 + 185 * 105\,906 * 1.219}{246\,805 * 1.119 + 105\,906 * 1.219} = 109.6℃$$

$$T_{14} = \frac{T_{FA} * \dot{m}_{FA,ESP,23} * Cp_{FA} + T_{13} * \dot{m}_{g,13} * Cp_{g,13}}{\dot{m}_{FA,ESP,23} * Cp_{FA} + \dot{m}_{g,13} * Cp_{g,13}}$$

$$T_{14} = \frac{10 * 5\,431 * 1.006 + 109.6 * 353\,395 * 1.101}{5\,431 * 1.006 + 353\,395 * 1.101} = 108.2℃$$

$$T_{15} = \frac{T_{FA} * \dot{m}_{FA,BF,24} * Cp_{FA} + T_{14} * \dot{m}_{g,14} * Cp_{g,14}}{\dot{m}_{FA,BF,24} * Cp_{FA} + \dot{m}_{g,14} * Cp_{g,14}}$$

$$T_{15} = \frac{10 * 7\,124 * 1.006 + 108.2 * 358\,827 * 1.101}{7\,124 * 1.006 + 358\,827 * 1.101} = 106.5℃$$

For stream 8 the gas composition is calculated using the AFM O_2 balance given in equation (3.31), while the H_2O concentration is calculated with equation (3.32). This way the H_2O concentration will be calculated based on raw material feed and gas flow rate for each run of the model.

$$y_{O_2,8} = \frac{y_{O_2,7} * \dot{V}_{g,7} + y_{O_2,FA} * \dot{V}_{FA,AFM,17}}{\dot{V}_{g,8}}$$

$$y_{O_2,8} = \frac{0.0451 * 80\,429 + 0.21 * 109\,252}{191\,075} = 0.1391$$

$$y_{H_2O,8} = \frac{y_{H_2O,7} * \dot{V}_{g,7} + \dot{V}_{H_2O,vap}}{\dot{V}_{g,8}}$$

$$y_{H_2O,8} = \frac{0.212 * 80\,429 + 1\,393}{191\,075} = 0.097$$

$$y_{CO_2,8} = \frac{y_{CO_2,7} * \dot{V}_{g,7}}{\dot{V}_{g,8}}$$

$$y_{CO_2,8} = \frac{0.1876 * 80\,429}{191\,075} = 0.079$$

Appendix K Process data plots

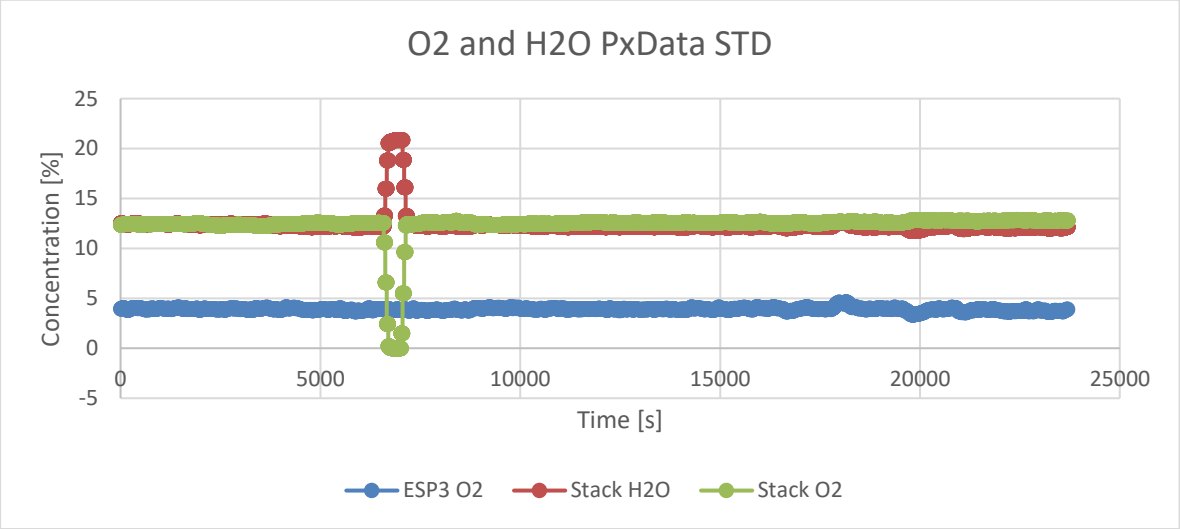

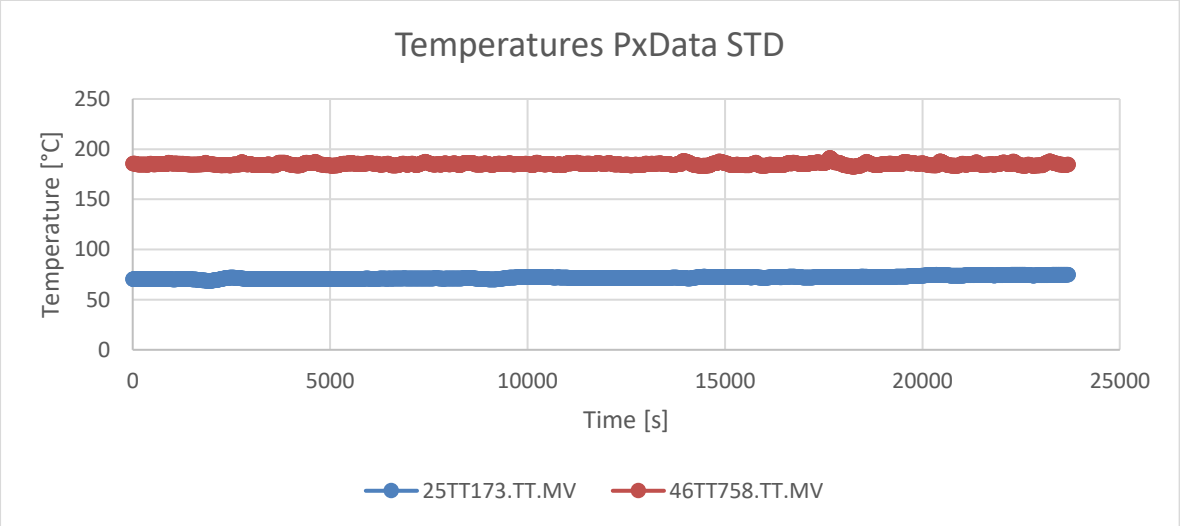

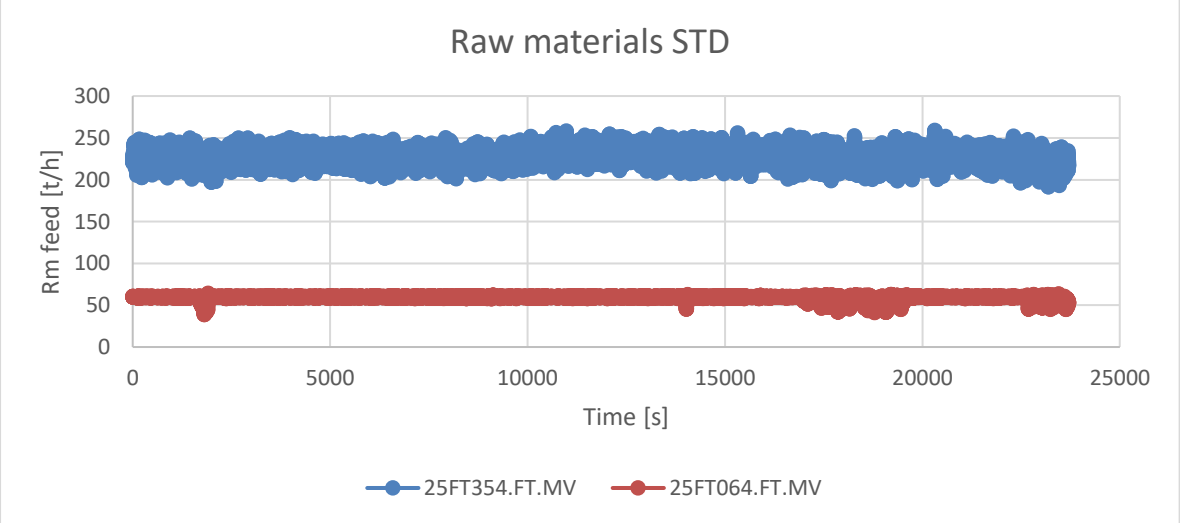

LA production

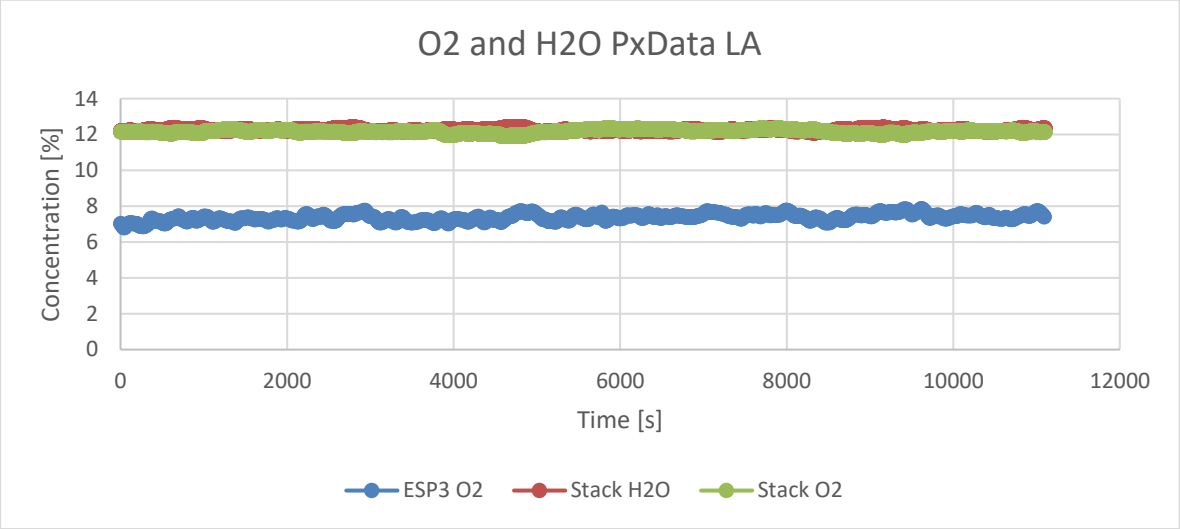

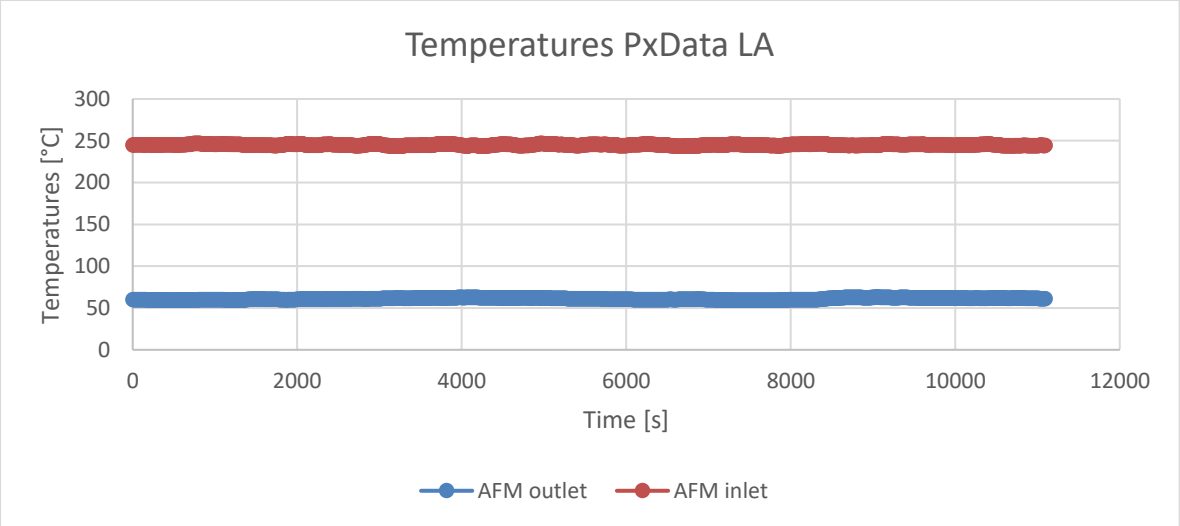

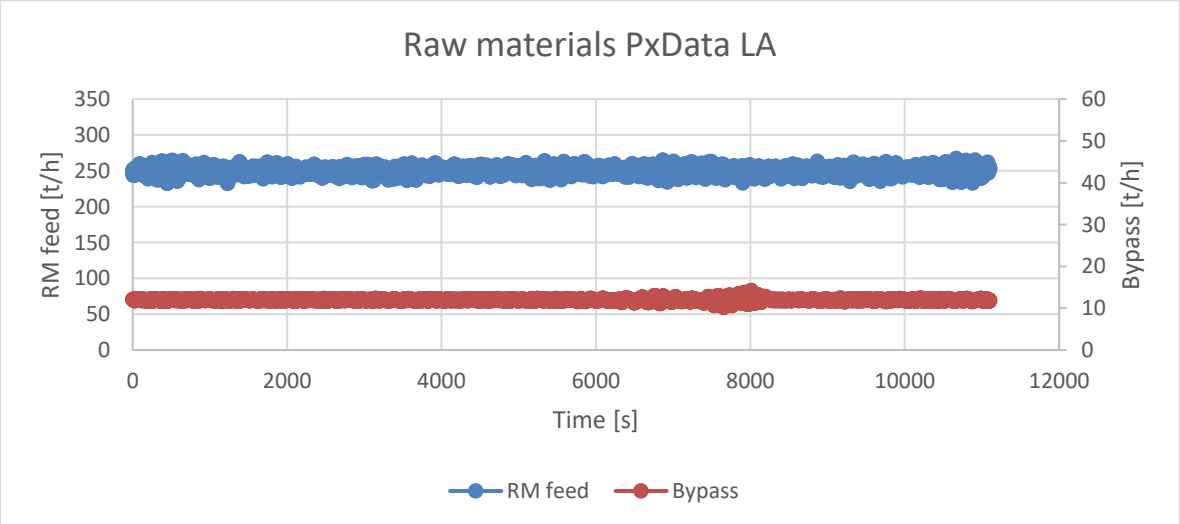

Appendix L Calculation of ESP3 O_2 online measurement deviance

First the volumetric flow rate is calculated based on the manual O_2 measurement in stream 1, and the online measurement downstream of the ESP3.

$$y_{O_2,ESP3} * \dot{V}_{g,ESP3} + y_{O_2,FA} * \dot{V}_{FA} = y_{O_2,1} * \dot{V}_{g,1}$$
$$\dot{V}_{FA} = \dot{V}_{g,1} - \dot{V}_{g,ESP3}$$

Combining these equations gives the following equation

$$y_{O_2,ESP3} * \dot{V}_{g,ESP3} + y_{O_2,FA} * \left(\dot{V}_{g,1} - \dot{V}_{g,ESP3}\right) = y_{O_2,1} * \dot{V}_{g,1}$$
$$0.0307 * \dot{V}_{g,ESP3} + 0.21 * \left(163\,368 - \dot{V}_{g,ESP3}\right) = 0.0451 * 163\,368$$

Then solving for the ESP3 gas flow before calculating the total false air intrusion.

$$\dot{V}_{g,ESP3} = 150\,247 Nm^3/h$$
$$\dot{V}_{FA} = 13121 Nm^3/h$$

Finally the new raw meal department inlet temperature is found

$$\dot{m}_{ESP3} * Cp_{g,1} * (T_{GCT} - T_1) = \dot{m}_{FA} * Cp_{FA} * (T_1 - T_{FA})$$
$$193841 * 1.219 * (185 - T_1) = 16986 * 1.006 * (T_1 - 10)$$
$$T_1 = 173°C$$

Appendix M Flowsheet STD production

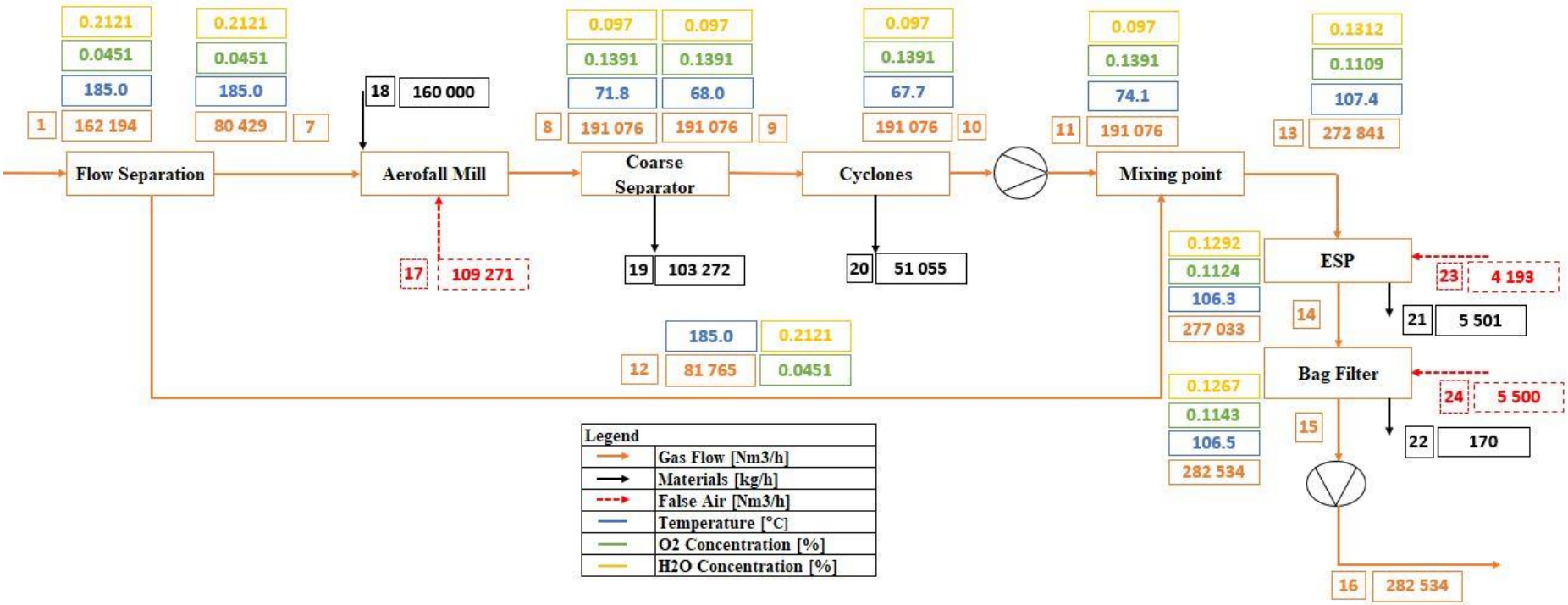

Appendix N Flowsheet LA production

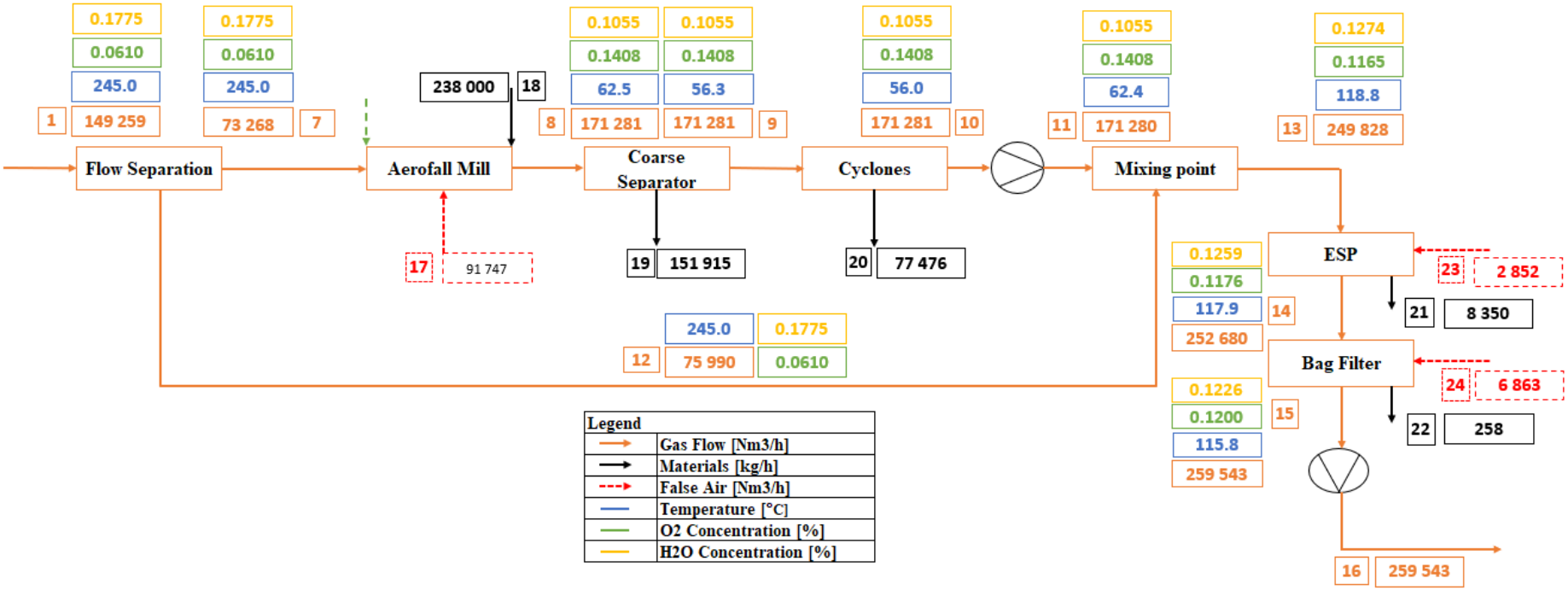

Appendix O Flowsheet STD production WHRU

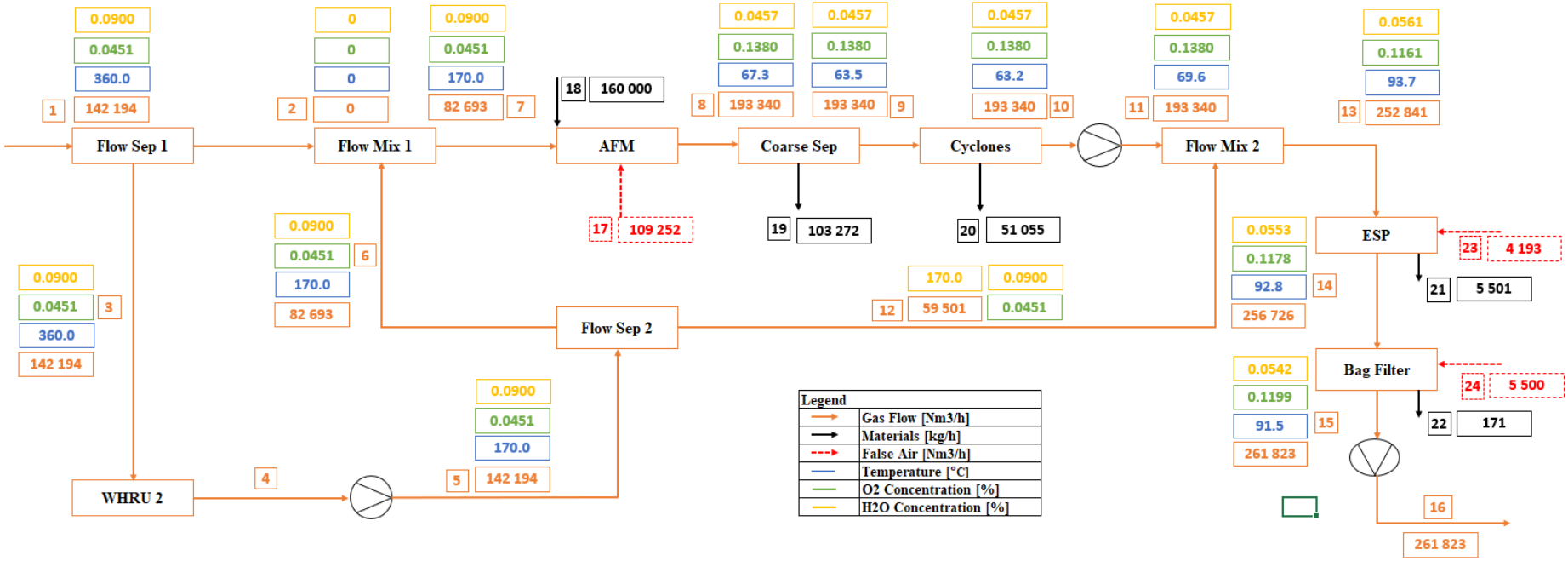

Appendix P Flowsheet LA production WHRU

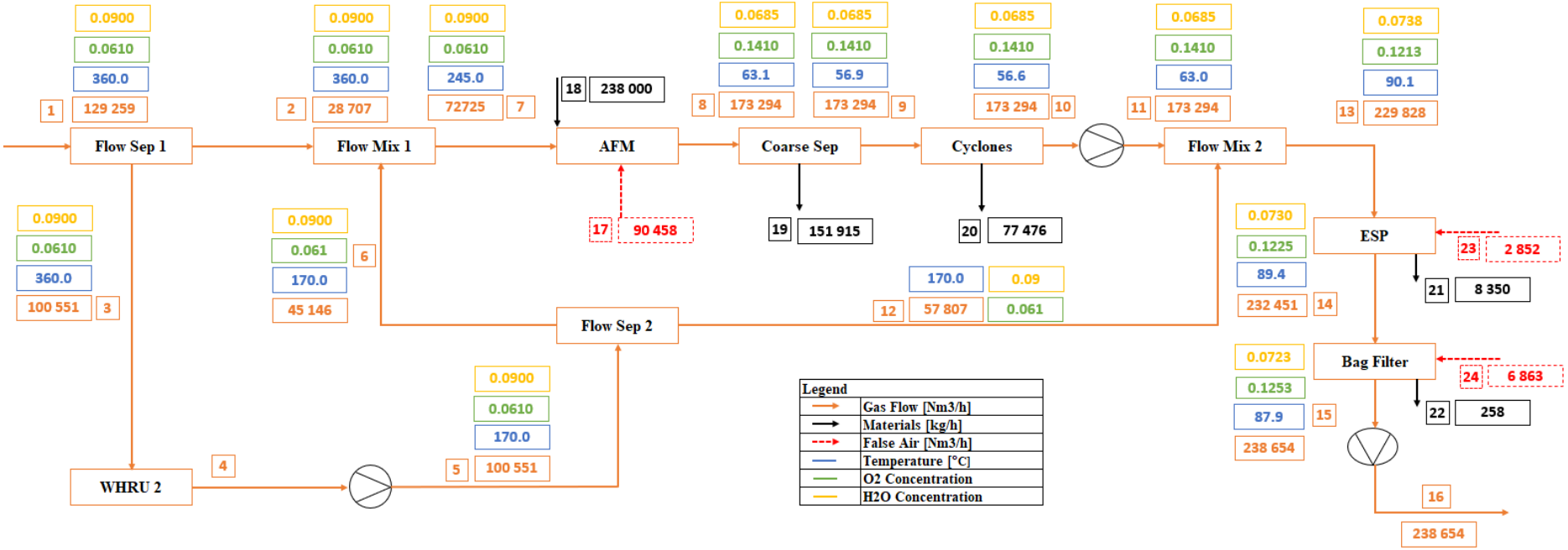

Appendix Q Flowsheet STD production WHRU reduced false air

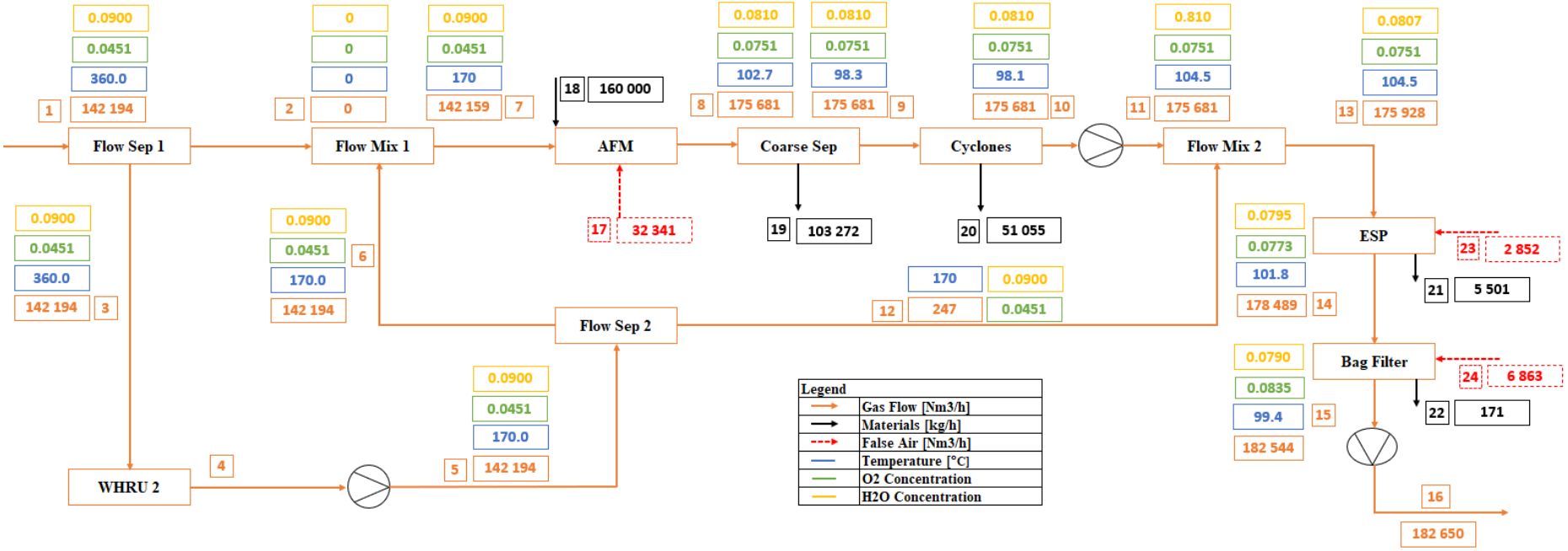

Appendix R Flowsheet LA production WHRU reduced false air

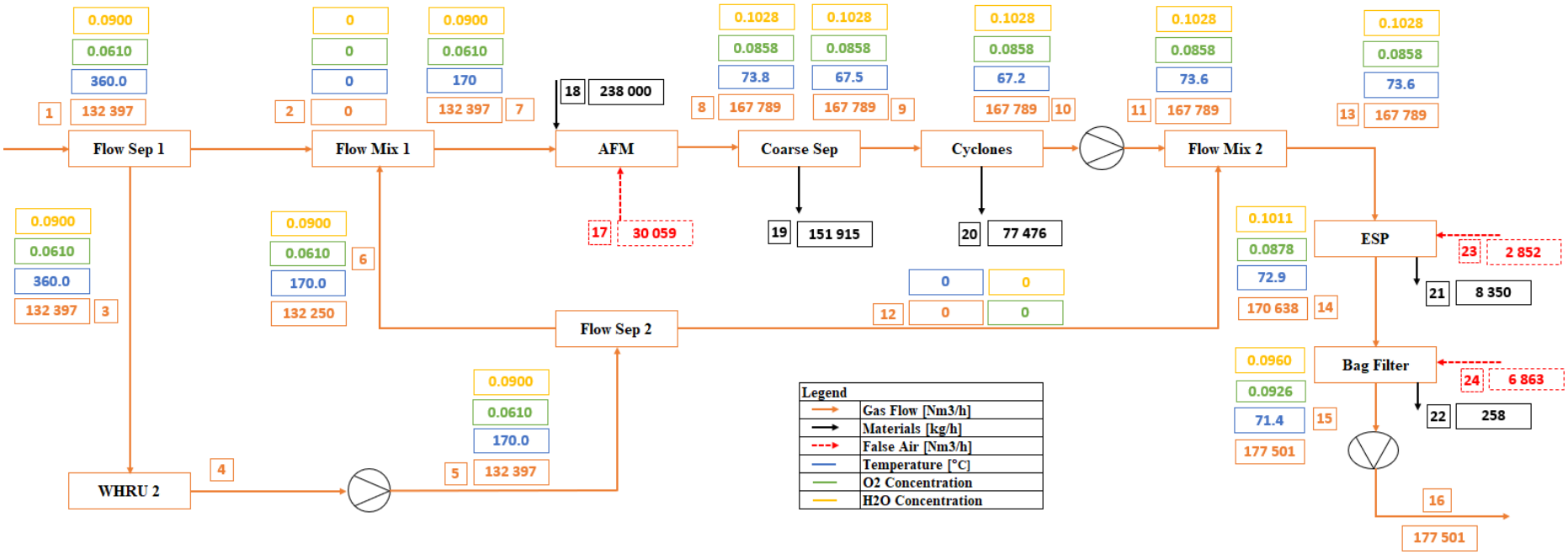

Appendix S Flowsheet LA production WHRU and reduced saturation temperature

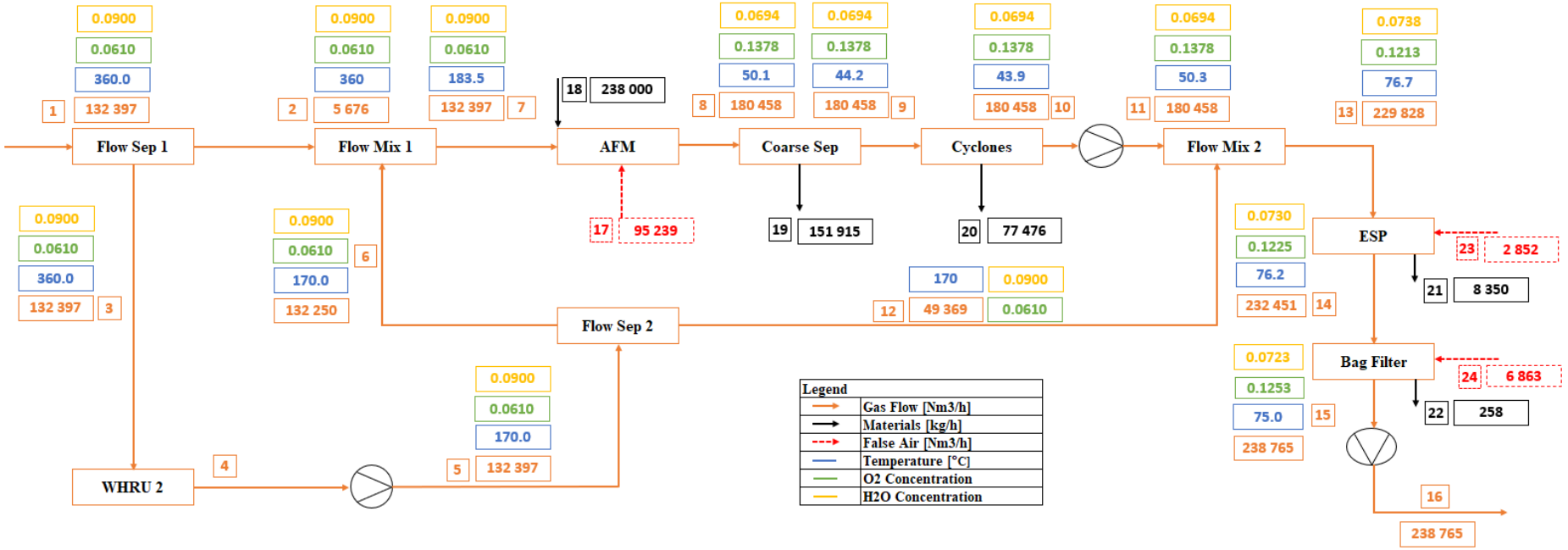

Appendices